Atmos. Chem. Phys. Discuss., https://doi.org/10.5194/acp-2018-724
Manuscript under review for journal Atmos. Chem. Phys.
Discussion started: 30 July 2018

Atmospheric Chemistry and Physics Discussions

Lagrangian simulations of the transport of young air masses to the top of the Asian monsoon anticyclone and into the tropical pipe

Bärbel Vogel[1], Rolf Müller[1], Gebhard Günther[1], Reinhold Spang[1], Sreeharsha Hanumanthu[1], Dan Li[1,2], Martin Riese[1], and Gabriele P. Stiller[3]

[1]Forschungszentrum Jülich, Institute of Energy and Climate Research - Stratosphere (IEK-7), Jülich, Germany
[2]Key Laboratory of Middle Atmosphere and Global Environment Observation (LAGEO), Institute of Atmospheric Physics, Chinese Academy of Sciences, Beijing, China
[3]Institute for Meteorology and Climate Research, Karlsruhe Institute of Technology, Karlsruhe, Germany

Correspondence: Bärbel Vogel (b.vogel@fz-juelich.de)

Abstract.

We have performed backward trajectory calculations and simulations with the 3-dimensional Chemical Lagrangian Model of the Stratosphere (CLaMS) for two succeeding monsoon seasons using artificial tracers of air mass origin. With these tracers we trace back the origin of young air masses (age $<$ 6 months) at the top of the Asian monsoon anticyclone and of air masses within the tropical pipe (6 months $<$ age $<$18 months) during summer 2008. The occurrence of young air masses ($<$6 months) at the top of the Asian monsoon anticyclone up to $\approx$460 K is in agreement with satellite measurements of chlorodifluoromethane (HCFC-22) by the Michelson Interferometer for Passive Atmospheric Sounding (MIPAS) instrument. HCFC-22 can be considered as a regional tracer for continental eastern Asia and the Near East as it is mainly emitted in this region.

Our findings show that the transport pathway of air masses from boundary sources in the region of the Asian monsoon into the tropical pipe occurs in three distinct steps. First, very fast uplift in 'a convective range' transports air masses up to 360 K potential temperature within a few days. Second, air masses are uplifted from about 360 K up to 460 K within 'an upward spiralling range' within a few months. The large-scale upward spiral extends from northern Africa to the western Pacific. The air masses are transported upwards by diabatic heating with a rate of up to 1–1.5 K per day, implying strong vertical transport above the Asian monsoon anticyclone. Third, transport of air masses occurs within the tropical pipe up to 550 K associated with the large-scale Brewer-Dobson circulation within $\sim$ one year.

In the upward spiralling range, air masses are uplifted by diabatic heating across the (lapse rate) tropopause, which does not act as a transport barrier under these conditions. Further, in the upward spiralling range air masses from inside the Asian monsoon anticyclone are mixed with air masses convectively uplifted outside the core of the Asian monsoon anticyclone in the tropical adjacent regions. However, this upward transport is weak in terms of transported air masses compared to the quasi-horizontal transport from the monsoon anticyclone into the northern lower stratosphere and tropical tropopause region. Air masses from the Asian monsoon anticyclone (India/China) contribute a minor fraction to the composition of air within the tropical pipe at 550 K (6%), the major fractions are from Southeast Asia (16%) and the tropical Pacific (15%) .

Atmos. Chem. Phys. Discuss., https://doi.org/10.5194/acp-2018-724
Manuscript under review for journal Atmos. Chem. Phys.
Discussion started: 30 July 2018

Atmospheric Chemistry and Physics Discussions

1 Introduction

The Asian summer monsoon is the most pronounced circulation pattern in boreal summer associated with deep convection over the Indian subcontinent and with an anticyclonic flow that extends from the upper troposphere into the lower stratosphere (UTLS) region (e.g., Li et al., 2005; Randel and Park, 2006; Park et al., 2007). The strong anticyclonic circulation in the UTLS acts as an effective transport barrier (e.g., Ploeger et al., 2015) causing a confinement of tropospheric trace gases in the anticyclone, isolating them from the surrounding air (stratospheric background) as shown by a variety of satellite measurements (e.g., Rosenlof et al., 1997; Li et al., 2005; Park et al., 2007; Fadnavis et al., 2014; Glatthor et al., 2015; Chirkov et al., 2016; Santee et al., 2017).

There is a large variability of the spatial extent, strength, and location of the UTLS anticyclone reaching from Northeast Africa to East Asia (e.g., Annamalai and Slingo, 2001; Randel and Park, 2006; Garny and Randel, 2013; Vogel et al., 2015; Pan et al., 2016). In particular, the location and the shape of the anticyclone change from day to day caused by the internal dynamical variability, manifesting in an oscillation between a state with one anticyclone and two separated anticyclones (2 modes) often referred as western (Iranian) and eastern (Tibetan) mode (e.g., Zhang et al., 2002; Vogel et al., 2015; Nützel et al., 2016). In addition, smaller anticyclones characterised by low PV values are breaking off a few times each summer from the main anticyclone, a process which is referred to as "eddy shedding" (Hsu and Plumb, 2001; Popovic and Plumb, 2001; Garny and Randel, 2013; Vogel et al., 2014, 2016; Ungermann et al., 2016).

The Asian monsoon circulation provides an effective pathway for tropospheric trace gases such as pollutants, aerosol precursors, or aerosols into the lower stratosphere which could play an important role in the formation of the Asian tropopause aerosol layer (ATAL) (e.g., Vernier et al., 2015; Höpfner et al., 2016). However, there is a longstanding debate about the transport mechanisms at the top of the Asian monsoon anticyclone and beyond into the stratosphere (e.g., Bannister et al., 2004; Park et al., 2009; Randel et al., 2010; Randel and Jensen, 2013; Bergman et al., 2012, 2013; Uma et al., 2014; Garny and Randel, 2016; Orbe et al., 2015; Tissier and Legras, 2016; Ploeger et al., 2017). Vertical upward transport into the deep stratosphere occurs within the tropical pipe, where tropical air masses are isolated to some extent from isentropic mixing with mid-latitude air (e.g., Plumb, 1996; Volk et al., 1996).

The transport of tropospheric trace gases by the Asian monsoon anticyclone into the lower stratosphere changes the chemical composition in this part of the Earth's atmosphere. Radiatively active species transported into the lowermost extra-tropical stratosphere have a significant impact on surface climate (e.g., Solomon et al., 2010; Riese et al., 2012; Hossaini et al., 2015) or can cause regional radiative forcing such as the ATAL layer (e.g., Vernier et al., 2015).

Here, we investigate the following two main questions: First, what are the transport pathways at the top of the Asian monsoon anticyclone into the stratosphere? Second, how do boundary layer source regions in Asia affect the composition of the lower/middle stratosphere within the tropical pipe?

To answer these questions we performed both backward trajectory calculations and three-dimensional simulations including irreversible mixing (Konopka et al., 2007) with the Lagrangian transport model CLaMS (McKenna et al., 2002b, a; Pommrich

Atmos. Chem. Phys. Discuss., https://doi.org/10.5194/acp-2018-724
Manuscript under review for journal Atmos. Chem. Phys.
Discussion started: 30 July 2018

Atmospheric Chemistry and Physics Discussions

et al., 2014, and references therein). Artificial tracers of air mass origin that mark defined regions in the Earth's boundary layer (covering the entire Earth's surface) are introduced in the CLaMS model (Vogel et al., 2015, 2016) and are compared to measurements of the Michelson Interferometer for Passive Atmospheric Sounding (MIPAS) instrument onboard the European Environmental Satellite (EnviSat) (Fischer et al., 2008; Chirkov et al., 2016) to study transport processes and pathways at the top of the Asian monsoon anticyclone and beyond into the tropical pipe. We conduct a case study for the monsoon season 2008. The monsoon season 2008 is chosen because MIPAS measurements have very good data coverage in summer 2008 over Asia. Further, in 2008 there was a normal monsoon season. It is established that a strong relation between El Niño and La Niña events in winter influence the rainfall abundance (droughts or floods) during the following Indian summer monsoon (e. g. Webster et al., 1998; Kumar et al., 2006). In winter 2007/08 (DJF), there was a strong La Niña according to the Oceanic Niño Index[1] causing a normal monsoon season in terms of medium rainfall over India in summer 2008[2].

We compare the distribution of tracers of air mass origin found in the CLaMS model with observations of global chlorodifluoromethane (HCFC-22; $CHClF_2$) measurements of the MIPAS satellite instrument (Chirkov et al., 2016). Chirkov et al. (2016) found enhanced values of HCFC-22 in the region of the Asian monsoon anticyclone at 16 km altitude in July, August, and September (JAS) averaged over the MIPAS measurement period from 2005 until 2011. In the last few decades, HCFC-22 has been used as a substitute for more potent ozone-depleting substances such as chlorofluorocarbons (CFCs) in the chemical industry, in particular as a refrigerant, in some regions of the Earth, e.g., in continental eastern Asia and in the Near East (Fortems-Cheiney et al., 2013; Simmonds et al., 2018). In contrast, the production and utilisation of HCFC-22 has been phased out in developed countries regulated by the Montreal Protocol and its amendments and adjustments. As a consequence, HCFC-22 is emitted in locally restricted regions, in particular in the region of the Asian monsoon. Simmonds et al. (2018) estimate that between 55% and 65% of the global HCFC-22 emissions within the last decade are from Chinese production.

Therefore, HCFC-22 is a good tracer for studying transport processes in the region of the Asian monsoon anticyclone and for comparing with CLaMS artificial tracers of air mass origin (e.g., Vogel et al., 2016). In this paper similar methods as in Vogel et al. (2016), namely three-dimensional CLaMS simulations with artificial tracers of air mass origin as well as MIPAS HCFC-22, are used, however the model setup and the scientific objectives are different. In Vogel et al. (2016) horizontal transport pathways out of the the Asian monsoon anticyclone between 360 K up to 400 K were analysed in a simulation for the monsoon season 2012. Vogel et al. (2016) found, in agreement with MIPAS HCFC-22 measurements, two main horizontal transport pathways from the Asian monsoon anticyclone: one to the east along the subtropical jet and subsequent transport into the northern lower stratosphere, a second horizontal transport pathway to the west into the tropical tropopause layer (TTL).

Here, a more sophisticated model setup is used with the focus on vertical transport pathways out of the Asian monsoon anticyclone and subsequent upward transport into the lower stratosphere up to 550 K. Two consecutive monsoon seasons in summer 2007 and 2008 are simulated. In this two-monsoon-season simulation, the different emission tracers are released during three different time periods each with a length of 6 months (i.e., we use a three-pulse-approach with a simulation period of 18 months). This allows as to infer the different transport times of air parcels from the Earth's surface to the top

[1] see e.g. http://ggweather.com/enso/oni.htm
[2] see e.g. http://www.tropmet.res.in/~kolli/mol/Monsoon/Historical/air.html

Atmos. Chem. Phys. Discuss., https://doi.org/10.5194/acp-2018-724
Manuscript under review for journal Atmos. Chem. Phys.
Discussion started: 30 July 2018

Atmospheric Chemistry and Physics Discussions

of the anticyclone and beyond in contrast to the approach of a one-monsoon-season simulation (one-pulse-approach with a simulation period of 6 months) used earlier (Vogel et al., 2015, 2016). With this approach it is possible to quantify the impact of the monsoon season of the year before (2007), the winter time 2007/2008, and the monsoon season 2008 on the lower stratosphere and in particular on the tropical pipe at the end of August 2008. This model setup allows us to identify the origin of air masses found at top of the Asian monsoon and within the tropical pipe as well as the transport times from the model boundary layer into the stratosphere including irreversible mixing processes.

2 CLaMS model simulations and MIPAS HCFC-22 measurements

We conduct model simulations with the three-dimensional chemistry transport model CLaMS (McKenna et al., 2002a, b; Pommrich et al., 2014, and references therein) and pure backward trajectory calculations with the CLaMS trajectory model covering the Asian monsoon season 2008.

The model simulations and trajectory calculations are driven by horizontal winds from ERA-Interim reanalysis (Dee et al., 2011) provided by the European Centre for Medium-Range Weather Forecasts (ECMWF). For the vertical velocities, the diabatic approach (with contributions to vertical velocities from radiative heating including the effects of clouds, latent heat release, mixing, and diffusion) was applied using diabatic heating rate as the vertical velocity including latent heat release (for details, see Ploeger et al., 2010). Further, CLaMS employs a hybrid vertical coordinate (ζ), which transforms from a strictly isentropic coordinate Θ to a pressure-based coordinate system (σ coordinates) below a certain reference level (in this study 300 hPa) (for more details, see Konopka et al., 2012; Pommrich et al., 2014). Previous studies demonstrated that the vertical transport in CLaMS allows the spatio-temporal distribution of CO within the Asian monsoon anticyclone measured by the Aura Microwave Limb Sounder (MLS) to be reproduced (Vogel et al., 2015; Ploeger et al., 2017).

2.1 Three-dimensional CLaMS simulations

The three-dimensional CLaMS simulations include irreversible mixing accounting for wind shear (Konopka et al., 2007) and are therefore capable of reproducing strong gradients of atmospheric trace gases found in regions with strong transport barriers, such as the edge of the Asian monsoon anticyclone (e.g., Konopka et al., 2010; Vogel et al., 2015, 2016; Ploeger et al., 2015, 2017), the extratropical tropopause in the vicinity of the subtropical jet (e.g., Pan et al., 2006; Vogel et al., 2011, 2016), and the polar vortex (e.g., Günther et al., 2008; Vogel et al., 2008).

The three-dimensional global CLaMS simulations employed here cover an altitude range from the surface up to 900 K potential temperature (≈ 37 km altitude) with a horizontal resolution of 100 km and a maximum vertical resolution of approximately 400 m near the tropopause. A two-monsoon-season simulation is performed covering the time period from 1 May 2007 to 31 October 2008, including both the 2007 and 2008 Asian monsoon seasons to study the upwelling of surface air characterised by local emissions into the lower stratosphere and into the tropical pipe during the course of two succeeding monsoon seasons.

Atmos. Chem. Phys. Discuss., https://doi.org/10.5194/acp-2018-724
Manuscript under review for journal Atmos. Chem. Phys.
Discussion started: 30 July 2018

Atmospheric Chemistry and Physics Discussions

In the two-monsoon-season simulation, artificial tracers of air mass origin, referred to as "emission tracers", that mark defined regions in the Earth's boundary layer (covering the entire Earth's surface) are implemented ($\approx$ 2–3 km above the surface following orography corresponding to $\zeta < 120$ K), as shown in Fig. 1 and Table 1. Within the model boundary layer, the sum of all the different emission tracers (Ω_i) is equal to 1 ($\Omega = \sum_{i=1}^{n} \Omega_i = 1$). Air masses in the model boundary layer are marked by different emission tracers every 24 hours (the time step for mixing in CLaMS) (for details see Vogel et al., 2016).

In the two-monsoon-season simulation, we used a three-pulse-approach and released the different emission tracers Ω_i in 3 different time periods (pulses) from t_j until $t_j + \Delta t_j$ with Δt_j equal to 6 months. For each pulse, the different emission tracers are continuously released (every 24 hours) at the model boundary between t_j and $t_j + \Delta t_j$. The three pulses start at 1 May 2007 for the summer/fall season 2007 (Summer 07 = S07; $\Omega_{\mathrm{S07}} = \sum_{i=1}^{n} \Omega_{i,\mathrm{S07}}$), 1 November 2007 for the winter/spring season 2007/2008 (Winter 07/08 = W07; $\Omega_{\mathrm{W07}} = \sum_{i=1}^{n} \Omega_{i,\mathrm{W07}}$), and 1 May 2008 for the summer/fall season 2008 (Summer 08 = S08; $\Omega_{\mathrm{S08}} = \sum_{i=1}^{n} \Omega_{i,\mathrm{S08}}$). The summer pulses were chosen to start a few weeks prior to the onset of the Asian monsoon. With this approach it is possible to quantify the impact of the monsoon season of the year before, namely Summer 07, on the lower stratosphere and in particular on the tropical pipe in summer 2008 in addition to the impact of younger air masses of Summer 08 (one-monsoon-season simulation) with an age lower than 6 months. Furthermore, with this approach also the impact of the strong upwelling above the Maritime Continent (the region between Indian and Pacific oceans) and the western Pacific (emission tracers for Southeast Asia and the tropical Pacific Ocean) during Winter 07/08 on the tropical pipe in summer 2008 is quantified.

In our two-monsoon-season simulation, the composition of an air mass in the free atmosphere (outside of the model boundary layer) will be a combination of air masses younger than 1 May 2007 ($\Omega_{\mathrm{S08}} + \Omega_{\mathrm{W07}} + \Omega_{\mathrm{S07}}$) and aged air masses ($A_{\mathrm{aged}}$) older than 1 May 2007 originating in the free troposphere or stratosphere ($\Omega_{\mathrm{S08}} + \Omega_{\mathrm{W07}} + \Omega_{\mathrm{S07}} + A_{\mathrm{aged}} = 1$).

In a one-monsoon-season simulation for the year 2012, Vogel et al. (2015) showed that the emission tracers for northern India plus southern India plus eastern China (in the following referred to as **'India/China'** tracer) are a good proxy for the location and shape of the Asian monsoon anticyclone using pattern correlations with potential vorticity (PV), and MLS O_3 and CO satellite measurements. Young air masses that are convectively uplifted outside the core of the Asian monsoon anticyclone and subsequently transported clockwise around the outer edge of the Asian monsoon mainly originate in Southeast Asia, the tropical Pacific, northwestern Pacific, and in northern Africa. Therefore, in this study the sum of these emission tracers is summarised in one emission tracer referred to as the tropical adjacent regions **'tropical AR'**. Note that in this paper a new emission tracer for the northwestern Pacific (NWP) is introduced in the CLaMS simulation compared to previous studies (Vogel et al., 2015, 2016) because it was demonstrated that tropical cyclones in the Pacific and their interaction with the Asian monsoon anticyclone play an important role in the chemical composition of air masses found at the edge of the anticyclone (Vogel et al., 2014; Li et al., 2017).

We note that also minor fractions of the emission tracers from the tropical adjacent regions (in particular from Southeast Asia) are found inside the Asian monsoon. This is due to the south-north shift and east-west oscillations of the monsoon anticyclone itself (Vogel et al., 2015).

Atmos. Chem. Phys. Discuss., https://doi.org/10.5194/acp-2018-724
Manuscript under review for journal Atmos. Chem. Phys.
Discussion started: 30 July 2018

2.2 CLaMS backward trajectory calculations

The three-dimensional CLaMS simulations including mixing simulate the contribution of different source regions within the model boundary layer to an air parcel in the free atmosphere. Pure trajectory calculations consider only the advective transport neglecting mixing processes entirely. However, backward trajectories are very well suited to analyse the detailed transport pathway of an air parcel and therefore provide an added value compared to three-dimensional CLaMS simulations (e.g., Vogel et al., 2014; Li et al., 2017).

Within this study, 20-day and 40-day backward trajectories are calculated using wind data from the ERA-Interim reanalysis (Dee et al., 2011) (with a horizontal resolution of $1° \times 1°$) to analyse the transport pathways of air parcels at the top of the Asian monsoon anticyclone and beyond into the tropical pipe.

2.3 Calculation of thermal tropopause

An accurate tropopause height determination is crucial to analyse to what extent the thermal tropopause acts as a vertical transport barrier at the top of the Asian monsoon anticyclone. In the extra-tropics, the tropopause acts as a chemical transport boundary in contrast to the tropics.

Here, we use an improved determination of the lapse rate tropopause for ERA-Interim data developed by Spang et al. (2015). The vertical resolution of the retrieved tropopause height cannot be better than the vertical grid resolution of the temperature data and hence can produce a significant positive bias for analyses with tropopause related altitude coordinates (Pan and Munchak, 2011). To partly compensate for this effect a vertical spline interpolation with 30 m vertical resolution is applied to the temperature profile around the actual tropopause height computed with the original vertical resolution. The tropopause height computation is repeated with the artificially higher vertical resolution and a weighted mean with distance of the four surrounding grid points of the observation point represents now the so-called high resolution tropopause height. This approach delivers a more realistic lapse rate tropopause, because the single tropopause height values are no longer associated to the altitude grid points of the analysis data anymore. Moreover, Spang et al. (2015) found with this approach smaller bias and standard deviation between ERA-Interim and radiosonde-based tropopause heights.

2.4 MIPAS HCFC-22 measurements

To compare the spatial distribution of CLaMS emission tracers with observations in the region of the Asia monsoon anticyclone, we compare results of the CLaMS simulation with global HCFC-22 measurements of the MIPAS satellite instrument (Data Version V5R) (Chirkov et al., 2016). HCFC-22 is emitted in locally restricted regions, in particular in the region of the Asian monsoon (Fortems-Cheiney et al., 2013; Simmonds et al., 2018), and is therefore very well suited for comparison with CLaMS emission tracers.

For MIPAS-CLaMS intercomparions, the data density of HCFC-22 measurements is improved by synoptic interpolation of multiple days of MIPAS measurements using CLaMS 3-dimensional trajectory calculations, making use of the relatively

long lifetime of HCFC-22 near the tropopause. For a specific day at the end of August 2008, trajectories were computed from the time of measurements in a time window of 4 days (i.e., ±2 days) to 12:00 UTC (Universal Time Coordinated) of the selected day. Over a period of a few days, there is practically no chemical destruction of HCFC-22 because of its global total atmospheric lifetime of about 12 years (SPARC Report 2013 'Lifetimes of Stratospheric Ozone-Depleting Substances', Ko et al., 2013).

A trajectory length of 2 days for the synoptical interpolation gives sufficient coverage of the MIPAS data in the region of the Asian monsoon. An even longer interpolation would give a higher data density, however by calculating solely trajectories mixing processes are neglected. Thus a time window of 4 days for the synoptical interpolation is a good compromise between sufficient data coverage and neglecting mixing processes.

The limited vertical resolution of the MIPAS HCFC-22 data needs to be taken into account in comparisons to model results. According to Chirkov et al. (2016), the vertical resolution is typically 3 km at 10 km altitude, linearly increasing to 7 km at 30 km altitude. At the altitudes relevant for this study, it is typically about 5 km (see Fig. 2 in Chirkov et al., 2016). However, given the rather smooth profiles expected in this study, the limited altitude resolution has a minor effect only; in contrast, it turns out to be crucial when highly structured profiles, such as typically occur at the edge of the polar vortex, are analysed. Further it has to be noted that tropical HCFC-22 profiles from MIPAS seem to have a high bias below 30 km, that, however, is broadly constant with altitude (Chirkov et al., 2016); thus, it does not affect the comparisons made here.

3 Results

3.1 Impact of emission tracers of the Summer 08 pulse

3.1.1 Contribution of different emission tracers to the top of the Asian monsoon anticyclone

To analyse the transport pathways at the top of the Asian monsoon anticyclone during the monsoon season 2008, we use only the tracers of air mass origin for the time pulse for Summer 08 (age $<$ 6 months).

The geographic position and shape of the Asian monsoon anticyclone have strong variability from day to day (e.g., Garny and Randel, 2013; Ploeger et al., 2015; Vogel et al., 2015). In this paper, we focus on 18 August 2008 during the monsoon season 2008 as a case study. On that day, the anticyclone has two modes, the western mode located over the Near East and the eastern Mediterranean Basin and the eastern mode over India and western China as shown in Fig. 2a. Further, a smaller anticyclone (eddy shedding event) is found over the northwestern Pacific. We selected the 18 August 2008 for this study because first this day is dynamically very interesting and second on this day there is very good data coverage of the MIPAS HCFC-22 measurements.

To analyse the transport of young air masses to the top of the Asian monsoon anticyclone, we distinguish between air masses that experienced strong upward transport mainly inside (India/China) and mainly outside (tropical adjacent regions) of the Asian monsoon anticyclone. Fig. 2 (top) shows the horizontal distribution of the fraction of the emission tracer for India/China (left) and for tropical adjacent regions (right) at 360 K potential temperature. It is evident in Fig. 2 (top) that

at 360 K the CLaMS model simulates very strong horizontal tracer gradients between the tracer for India/China and for the tropical adjacent regions at the edge of the anticyclone. High fractions of air from India/China up to 90% and low fractions below 10% from the tropical adjacent regions are found in the core of the Asian monsoon anticyclone at 360 K potential temperature. Highest fractions from the tropical adjacent regions of about 40% are found in a belt around the edge of the anticyclone. Towards the north this belt is separated by the subtropical jet from the northern lower stratosphere visible as a very sharp gradient. To the south, air masses from the tropical adjacent regions do not show a strong gradient with air masses within the tropics and therefore are not separated by a strong transport barrier from the TTL at a level of potential temperature of 360 K.

In this paper, we define inside and outside (= outer edge or belt of) the anticyclone using these simulated horizontal gradients of the tracers for India/China and for tropical adjacent regions at 360 K. In the following, we will show that this separation is not valid for higher levels of potential temperature.

Fig. 2 (2nd row) shows the longitude–theta cross sections at 25°N of the fraction from India/China (left) and from the tropical adjacent regions (right) on 18 August 2008. We would like to emphasise the horizontal transport of air masses with high fractions from India/China (40%–90%) from the eastern part of the anticyclone to both the western part and into the eddy over the western Pacific between 350 K and 380 K. Correspondingly, low values of the tropical adjacent regions (0%–30%) are simulated in these regions.

Fig. 2 shows the latitude–theta cross sections in the eastern mode of the anticyclone at 90°E (3rd row) and in the western mode of the anticyclone at 30°E (bottom) on 18 August 2008. Below 360 K, high fractions of air from India/China up to 90% and low fractions from the tropical adjacent regions lower than 5% are found in the eastern mode of the anticyclone. In the western mode there is still a high fraction from India/China between 30% and 60% and 10%–40% from the tropical adjacent regions.

Further, a strong vertical gradient of the India/China tracer is found at about 360 K. This level is below the thermal tropopause, which is located at around 380 K ($\approx$ 100 hPa) over the eastern mode of the Asian monsoon anticyclone (at 90°E). There is a layer of young air masses with enhanced fractions from India/China (up to $\approx$ 20%) above the thermal tropopause up to about 420 K potential temperature. An obvious explanation for this model result would be that the tropopause over the Asian monsoon is not a strict vertical transport barrier and weak vertical cross-tropopause transport occurred, in contrast to the extra-tropics (air masses at the polar side of the subtropical jet) where the tropopause acts as a chemical transport boundary.

Inside the anticyclone below 360 K, the fractions from the tropical adjacent regions are below 10%, however above 360 K around the tropopause the fractions are much higher, up to about 35%, and up to about 15% around 420 K. Thus, at 420 K the contributions of young air masses are about 20% from India/China and 15% from the tropical adjacent regions. From this result the question arises, 'how can air masses from the outer edge of the anticyclone be transported from 360 K into the lower stratosphere above?' A straight vertical cross-tropopause transport cannot be the explanation because inside the anticyclone the fraction from the tropical adjacent regions is much lower.

Atmos. Chem. Phys. Discuss., https://doi.org/10.5194/acp-2018-724
Manuscript under review for journal Atmos. Chem. Phys.
Discussion started: 30 July 2018

3.1.2 Emission tracer for India/China vs MIPAS HCFC-22

To demonstrate that the spatial distribution of tracers of air mass origin found in the CLaMS model in the region of the Asian monsoon anticyclone is consistent with observations of chemical tracers, we analyse HCFC-22 measurements of the MIPAS instrument (Chirkov et al., 2016). As described in Sect. 1, HCFC-22 is emitted in locally restricted regions in particular in continental eastern Asia, in particular in China, and in the Near East.

Fig. 3 (top) shows the horizontal distribution for the India/China tracer (left) and of HCFC-22 measurements (right) synoptically interpolated to 18 August 2008 12:00 UTC at 380 K potential temperature (for details see Sect. 2.4) and latitude–theta cross sections (2nd row) at 30°E ± 10° and 90°E ± 10° as well as a longitude–theta cross section at 25°N (bottom). The contour line of 20% for percentages of the India/China tracer are marked for better comparison with the CLaMS results shown in Fig. 2.

The horizontal spatial distribution of the India/China tracer and HCFC-22 at 380 K show good overall agreement. In particular the strong gradient at the northern flank of the Asian monsoon anticyclone is evident both in the model and in HCFC-22 observations. Enhanced HCFC-22 values up to 240 pptv compared to the stratospheric background (of around 180 to 200 pptv at 16 km altitude in JAS derived from MIPAS measurements (Chirkov et al., 2016)) are found in both the eastern and western mode of the anticyclone, in the smaller eddy at the northeastern flank of the anticyclone as well as in the thin filament at around 50°E between 40°N and 60°N. Further, as in the CLaMS model in the observations there is no sharp gradient at the southern flank of the anticyclone, which separates anticyclonic air from the surrounding tropics.

The vertical HCFC-22 distributions (Fig. 3, 2nd row) within the eastern and western mode of the anticyclone are consistent with the vertical distribution of the India/China tracer (see Fig. 2e,g). The highest mixing ratios of HCFC-22 are found within the anticyclone below the thermal tropopause. However, also at the top of the anticyclone above the tropopause enhanced HCFC-22 values are measured in agreement with the CLaMS tracer for India/China. Thus, measurements of HCFC-22 are consistent with our model result that young air masses from the region of the Asian monsoon are transported to the top of the anticyclone above the tropopause.

In addition, the vertical HCFC-22 distribution (Fig. 3, 2nd row left) for the western mode shows a very steep gradient in the upper troposphere between 350 K and 360 K in agreement with the spatial distribution of the India/China tracer (see Fig. 2g). Thus below 350–360 K lower mixing ratios of HCFC-22 are measured than above, indicating that below the western mode of the anticyclone there exists no upward transport from boundary sources for HCFC-22. The enhanced values of HCFC-22 within the western mode and below the thermal tropopause along the longitude–theta cross sections at 25°N (Fig. 3, bottom) confirm the horizontal westward transport within the Asian monsoon anticyclone as found for the India/China tracer in the CLaMS simulations (see Fig. 2c).

Atmos. Chem. Phys. Discuss., https://doi.org/10.5194/acp-2018-724
Manuscript under review for journal Atmos. Chem. Phys.
Discussion started: 30 July 2018

3.1.3 Impact of young air masses on the top of the AMA

In Sect. 3.1.1, it is shown that enhanced fractions of both tracers for India/China and tropical adjacent regions are found above the thermal tropopause at the top of the Asian monsoon anticyclone. Fig. 4 shows the horizontal distribution of the fraction of air originating in India/China (left) and in tropical adjacent regions (right) at different levels of potential temperature between 380 K and 460 K.

Young air masses (age $<$ 6 months) from both India/China and tropical adjacent regions are found up to ≈460 K. At 380 K, the highest fractions of air from India/China are found in the core of the anticyclone and of the tropical adjacent regions at the edge of the anticyclone. At 400 K, the highest contributions of both tracers are found within the anticyclone; however, between 420 K and 460 K highest contributions of both are found around the edge of the anticyclone. This is an indication that at these altitudes the vertical upward transport of young air masses occurred more at the edge of the anticyclone and not inside the anticyclone itself.

3.2 Backward trajectory calculations

3.2.1 40-day backward trajectories at the top of the anticyclone and beyond

To analyse the transport pathways to the top of the anticyclone in more detail, 40-day backward trajectories are calculated started in the western (20–50°N,0–70°E) and eastern (20–50°N,70–140°E) mode of the anticyclone at different levels of potential temperature ($\Theta \pm 0.25\,K$). Only air parcels are selected with contributions of young air masses (age $<$ 6 months, Summer 08) larger than 70% (380 K), 50% (400 K), 20% (420 K), and 5% (440 K) (not all levels of potential temperature are presented within this paper). The results of all 40-day backward trajectories are similar; therefore we show a selection of trajectories to demonstrate the transport pathways at the top of the Asian monsoon.

Fig. 5 shows trajectories started in the western part of the Asian monsoon anticyclone around the thermal tropopause at 380 K. Air masses are uplifted to approximately 360 K very rapidly by various convective events occurring at different times and locations. Our 40-day backward trajectories show that preferred regions for fast uplift are the Tibetan Plateau and the western Pacific.

The backward trajectories demonstrate that above 360 K potential temperature the air masses circulate around the anticyclone in a large-scale upward spiral extending from northern Africa to the western Pacific. Here in the upward spiralling range, the upward transport is much slower than in the convective range.

Fig. 6 shows trajectories started in the western and eastern part of the Asian monsoon anticyclone above the thermal tropopause at 400 K and at 440 K. The slow upward transport up to ≈ 1 to 1.5 K per day in a large-scale upward spiral is evident in both the western and eastern part. The 40-day backward trajectories demonstrate that at the top of the anticyclone the upward transport of air masses occurs along a large-scale upward spiral and therefore no straight vertical upward transport from the upper tropopause into the lower stratosphere takes place. The higher above the thermal tropopause the larger is the contribution of trajectories from outside the Asian monsoon anticyclone coming into the upward spiralling flow above 360 K. Trajectories at other levels of potential temperature (not shown) both in the western and in eastern part of the anticyclone have

a similar behaviour as shown in Figs. 5 and 6 and therefore confirm the presented results.

3.2.2 Global 20-day backward trajectories in the region of the Asian monsoon anticyclone

In the last section, the transport pathways of single selected trajectories were discussed. Here, for a broader view 20-day backward trajectories for the entire region of the Asian monsoon anticyclone are presented. In the region of the Asian monsoon (0–160°E and 10–60°N) on a $1.0° \times 0.5°$ longitude-latitude-grid 20-day backward trajectories are calculated at 360 K, 380 K, 400 K, 420 K, and 440 K starting on 18 August 2008. Each point in Fig. 7 indicates the location of the start position of a 20-day backward trajectory colour-coded by the change in potential temperature ($\Delta\Theta$) during the last 20 days.

At 360 K, air parcels that experienced very strong upward transport by up to ≈ 60 K within the last 20 days were found inside the western and eastern mode of the anticyclone, within the eddy over the Pacific, and within the tropics south of the anticyclone. The upwelling is very patchy, reflecting that the strong upward transport in this region is caused by single convective events.

Above 360 K, air parcels that experienced substantial upward transport are only found in the region of the anticyclone, however the upwelling is inhomogeneous and slow, with an uplift of about a maximum of 1–1.5 K per day. Air parcels that experienced upward transport are mainly grouped in curved elongated filaments, reflecting a rotating movement of the air parcels at the top of the anticyclone. Often air parcels with maximum $\Delta\Theta$ above 360 K are located more at the edge of the eastern and western mode of the anticyclone and at the edge of the eddy. This is consistent with results presented above in Sect. 3.2.1 demonstrating that for single selected trajectories the transport at the top of the Asian monsoon anticyclone is a slow upward transport of about 1–1.5 K per day in a large-scale spiral above the anticyclone caused by diabatic heating. In backward trajectory calculations mixing processes are not included, however the results of the trajectory calculations are consistent with patterns found in the 3-dimensional CLaMS simulation including mixing as discussed in Sect. 3.1.3, demonstrating that young air masses above 400 K are found at the edge of the anticyclone.

In Appendix A, results of global 20-day backward trajectories demonstrate that during the monsoon season above 360 K an uplift of air parcels of about 1–1.5 K per day occurred only in the region of the Asian monsoon anticyclone compared to the rest of the tropics. Even in the tropics the uplift is in general slower at these levels of potential temperature. Further the seasonal variability of this upwelling above the Asian monsoon anticyclone from monsoon-onset until post-monsoon 2008 is discussed in the Appendix A.

3.3 Results from the three-pulse-approach

In the previous sections, we could show that the Asian monsoon is an effective circulation pattern in the UTLS that transports very young air masses ($<$ 6 months) from the surface into the lower stratosphere up to ≈ 460 K. Here, we discuss subsequent

transport pathways of air masses from the region of the Asian monsoon and Southeast Asia into the tropical pipe (middle stratosphere).

3.3.1 Transport within the tropical pipe

Fig. 8 shows latitude–theta cross sections at 90°E for the fraction from India/China from the start of the simulation on 1 May 2007 until 18 August 2008, which is a sum of the contributions of each of the three time pulses Summer 07, Winter 07/08, and Summer 08 each set for a time period of 6 months. A signal with enhanced fractions from India/China (up to 10%) is found at around 550 K within the tropics which is from the Summer 07 pulse. This shows that air masses from boundary regions in India/China are transported into the middle stratosphere within the tropical pipe within a time period of one year. No fractions from India/China for the time pulse for Winter 07/08 are found on 18 August 2008, demonstrating that during winter time in the absence of the Asian monsoon anticyclone no boundary emissions from India/China are transported into the stratosphere.

Fig. 9 shows the same images as Fig. 8, but for the fractions from Southeast Asia (SEA). Because of the Summer 08 pulse, high fractions from Southeast Asia are found at the edge of or outside the Asian monsoon anticyclone below 360 K. At altitudes up to ≈460 K, enhanced fractions are found over the region of the Asian monsoon, but also above the entire tropics.

For the Summer 07 pulse, an enhanced signal from Southeast Asia (up to 25%) is found at around 550 K within the tropics similar as for India/China tracer. This model result shows that also air masses from outside the Asian monsoon anticyclone (Summer 07 pulse) are transported into the middle stratosphere within the tropical pipe within one year. The fraction of air from Southeast Asia (up to 25%) is even larger as from India/China (up to 10%). In contrast to the India/China tracer (Winter 07/08 pulse), the Southeast Asia tracer shows that also emissions from Southeast Asia released during winter time (Winter 07/08 pulse) are transported into the lower stratosphere via the tropical pipe.

Fig. 10 shows that the upward spiralling transport above 360 K occurs in a field of radiative heating above the Asian monsoon, in particular above the western mode of the anticyclone. Thus, the combination of the anticyclonic flow and the uplift by radiative heating results in an upward spiralling transport like a ‘Spiral Staircase’. Positive radiative heating rates are found in Era-Interim analysis on top of the Asian monsoon anticyclone as well as over the subtropics in the southern hemisphere (see Fig. 10). In these regions, positive radiative heating rates were also reported in a study by Park et al. (2007), using a free-running climate model. They argue that the positive radiative heating rates are the response to very low temperatures around the tropopause which again are the response to convective heating near the equator (e.g., Gill, 1980; Highwood and Hoskins, 1998). It is known that the radiative heating rates in the tropical UTLS are different in current reanalysis models (e.g., Wright and Fueglistaler, 2013) and are most likely overestimated in ERA-Interim (e.g., Schoeberl et al., 2012).

Fig. 11 shows MIPAS HCFC-22 measurements at the same longitude–theta cross sections as Fig. 9 and Fig. 8. The transport pathway of HCFC-22 within the tropical pipe is evident. The transport of HCFC-22 is similar to that of the emission tracer for Southeast Asia, in contrast to the signal for the India/China tracer, which results from a combination of two signals, one from the Summer 07 pulse and another from Summer 08 pulse. It was shown in previous studies (Chirkov et al., 2016; Vogel et al., 2016) that HCFC-22 is enhanced in the region of the Asian monsoon anticyclone. There are also HCFC-22 source regions outside the Asia monsoon region in continental eastern Asia (Fortems-Cheiney et al., 2013), therefore the upward transport

Atmos. Chem. Phys. Discuss., https://doi.org/10.5194/acp-2018-724
Manuscript under review for journal Atmos. Chem. Phys.
Discussion started: 30 July 2018

of HCFC-22 in the troposphere can also occur during winter time. In boreal winter, efficient transport into the stratosphere is found over the west Pacific and Maritime Continent caused by strong convection and in addition by the ascending branch of the Walker Circulation located over the Maritime continent (e.g., Bergman et al., 2012; Hosking et al., 2012). In addition, stronger heating rates (vertical velocity) are found in the TTL during winter compared to summer time (e.g., Bergman et al., 2012).

Figs. 8, 9, and 11 further show that in addition to the upward transport into the tropical pipe, horizontal transport pathways exists; that transport air masses isentropically out of the region of the Asian monsoon into the northern lower stratosphere and to a much lower extent into the southern hemisphere. These quasi-horizontal transport pathways are further discussed in Sect. 4.

3.3.2 Transport times and origin of air within the tropical pipe

On 18 August 2008, enhanced signals for the tracers from India/China and Southeast Asia from the Summer 07 pulse are found at around 550 K in the tropics between 30°S and 30°N (Fig. 12). To analyse in more detail the transport times from the model boundary into the tropical pipe the contributions of the three different time pulses from different emission tracers are calculated within the tropical pipe at 550 K potential temperature. We use the following approach: for each day between 1 May 2007 and 31 October 2008, a mean value for each emission tracer of all CLaMS air parcels is calculated between 30°S and 30°N at 550 K ($\pm$ 0.5 K). This is done for the sum of all three time pulses Summer 07, Winter 07/08, and Summer 08 and for each pulse individually.

Fig. 12 (top) shows the contribution of the three different time pulses (Ω_{S07}, Ω_{W07}, Ω_{S08}) for the entire Earth's surface between 1 October 2007 until the end of the simulation period (31 October 2008). The time period between 1 May 2007 and 1 October 2007 is not shown because here the contribution of all emission tracers is zero caused by the fact that the air masses need a certain transport time to reach the level of 550 K potential temperature within the tropical pipe. Air masses from the Summer 07 pulse reach this level first in November/December 2007; between January and May there is a steep increase of air masses from the Summer 07 pulse with a maximum in June 2008. Air masses from the Winter 07 pulse reach the 550 K level of potential temperature during May 2008 and are increasing until the end of the simulation period. No contributions from the Summer 08 pulse are found at 550 K, since the transport times are too short to reach the tropical pipe within the simulation period.

The highest contributions to the Summer 07 pulse are from tropical Pacific, India/China, Southeast Asia, and northern Africa Fig. 12 (top). To the Winter 07 pulse contribute mainly the tropical Pacific and Southeast Asia. Here, the contribution of India/China and northern Africa is insignificant, demonstrating that during the absence of the monsoon anticyclone in winter no vertical transport into the tropical pipe occurred.

Fig. 12 (bottom) shows that on the 550 K level, the contributions of all boundary emission tracers (age $<$ 18 months) to the tropical pipe is up to 55% by the end of October 2008. The contributions from Southeast Asia and the tropical Pacific are 16% and 15%, respectively. The contribution from India/China, which is mostly monsoon air, is much lower, around 6%. Lower fractions are from tropical Indian Ocean (4%), Northern Africa (3%), and South America (4%). The contributions of all other

regions of the Earth's surface are lower than 3% and are summarised in the tracer referred to as residual surface (8%) shown in grey.

The black and the white lines in Fig. 12 (bottom) mark the the contribution of the Summer 07 and Winter 07/08 pulses for each emission tracer, respectively (as shown in Fig. 12 (top)). For the tracer from India/China as well as for northern Africa, the black and the white lines are overlapping, implying that there is no contribution from India/China or northern Africa from the Winter 07/08 pulse in the tropical pipe (as shown above). Further, our findings show that air masses from the Asian monsoon anticyclone contribute to a lower fraction of the composition of air within the tropical pipe at 550 K; the major part is from Southeast Asia and the tropical Pacific. We would like to point out that CLaMS emission tracer for Southeast Asia include both the land masses of Southeast Asia and parts of the western Pacific including the Maritime Continent, which is known to also have intense deep convection during summer (e.g., Pan and Munchak, 2011).

4 Discussion

It has been proposed that the Asian monsoon anticyclone constitutes an effective transport pathway from the surface, through the Asian monsoon, and deep into the tropical pipe using satellite observations of hydrogen cyanide (HCN) (Randel et al., 2010). HCN is a tropospheric pollutant produced by biomass burning with a strong sink on ocean surfaces. Therefore tropical ocean regions cannot be the source for HCN found in the tropical pipe. Ploeger et al. (2017) confirm using CLaMS simulations marking air masses within the Asian monsoon anticyclone by a PV-gradient criterion (Ploeger et al., 2015) that the air mass fraction from the anticyclone correlates well with satellite HCN within the tropical pipe.

In our study, we found a similar behaviour for contributions of the India/China tracer within the tropical pipe as Randel et al. (2010) and Ploeger et al. (2017) for HCN and the simulated anticyclone air mass fraction. However in addition, we show that the contributions from emissions from Southeast Asia and the tropical Pacific during summer are larger than the contribution from India/China within the tropical pipe. This demonstrates that the Asian monsoon anticyclone is a more effective transport pathway for the tropical adjacent regions from which air masses can be transported to the edge of the Asian monsoon anticyclone and then further into the tropical pipe than for air masses from inside the anticyclone itself (India/China).

It has been demonstrated by satellite observations that the Asian monsoon anticyclone affects the transport of sulphate aerosol and its precursor SO_2 injected by volcanic eruptions within the adjacent regions of the Asian monsoon (e.g., Bourassa et al., 2012; Griessbach et al., 2013; Fairlie et al., 2014; Fromm et al., 2014; Wu et al., 2017). However, there is a debate about the exact transport mechanism. The observed transport into the stratosphere of air masses injected into the upper troposphere by volcanoes located at the edge of the Asian monsoon (e.g., Griessbach et al., 2013; Fairlie et al., 2014; Fromm et al., 2014; Wu et al., 2017) can be explained by the vertical transport concept of upward spiralling above the the Asian monsoon, proposed here. It has been found in several satellite measurements (Griessbach et al., 2013; Fromm et al., 2014; Fairlie et al., 2014) that polluted air masses from the Nabro eruption in Eritrea, northeastern Africa, in June 2011 are transported around the anticyclone and at higher levels are found above the anticyclone, consistent with the CLaMS tracer for the tropical adjacent regions. Wu

et al. (2017) show that the Asian monsoon anticyclone causes the transport of air masses emitted by the June 2009 eruption of the volcano Sarychev around the anticyclone southwards into the TTL, isolating aerosol-free air masses inside the anticyclone from aerosol-rich air outside.

Furthermore, the concept of the upward spiralling range transporting air masses from the adjacent regions of the Asian monsoon can also explain the impact of air masses uplifted by tropical cyclones in the western Pacific ocean on air masses observed by balloon measurements over Lhasa (China) (Li et al., 2017). Tropical cyclones rapidly loft marine air masses outside the Asian monsoon into the upper troposphere. The interplay between the location of the Asian monsoon antiyclone and the tropical cyclone controls the transport pathways of the air parcels from the boundary layer. Air parcels injected by a tropical cyclone into the outer anticyclonic flow of the anticyclone follow the flow around the anticyclone.

Moreover, the concept of the upward spiralling range including air mass transport from sources in the tropical adjacent regions could be a transport pathway to understand the formation of the Asian tropopause aerosol layer (ATAL) (e.g., Vernier et al., 2015) observed above the Asian monsoon region (Hanumanthu et al., 2018, in preparation).

However, we would like to emphasise that this vertical transport of air masses is much slower than the horizontal isentropic transport by eastward eddy shedding events transporting air from the Asian monsoon anticyclone and from the tropical adjacent regions into the northern lower stratosphere or westward shedding transporting air into the TTL (e.g., Garny and Randel, 2016; Orbe et al., 2015; Vogel et al., 2016; Ploeger et al., 2017). The impact of the quasi-horizontal transport on the chemical composition of the northern lower stratosphere is already discussed in detail in previous studies (e.g., Dethof et al., 1999; Ploeger et al., 2013; Müller et al., 2016; Vogel et al., 2014, 2016; Rolf et al., 2018).

Vogel et al. (2016) performed a CLaMS simulation for the year 2012 using similar tracers of air mass origin as in this work and found a flooding of the lower northern stratosphere with young air masses from the region of the Asian monsoon anticyclone. Horizontal transport of young air masses (age < 6 months) is calculated, resulting in up to 44% at 360 K (up to 35% at 380 K), with the highest contribution from India/China up to 15% (14%) (see Fig. 14 in Vogel et al. (2016)). In this paper, the same analysis is performed for the simulation for 2008 and a slightly higher impact on the extratropical northern lower stratosphere is found for the year 2008, up to 48% young air at 360 K (up to 41% at 380 K) and up to 18% (16%) from India/China compared to 2012 (see Appendix B). This difference is most likely caused by the interannual variability of the monsoon system. However, within the tropical pipe at 550 K, in 2008 the contributions from India/China are much smaller than 10 %, demonstrating that the horizontal isentropic transport of air masses from the Asian monsoon anticyclone into the stratosphere is more effective than the vertical transport.

5 Conclusions

In this paper, the transport mechanisms of young air masses at the top of the Asian monsoon and subsequent transport into the tropical pipe are analysed using 3-dimensional CLaMS simulations as well as CLaMS backward trajectory calculations. Tracers of air mass origin are introduced in the 3-dimensional CLaMS simulation to trace back the origin of young air masses

(age < 6 months) found at the top of the Asian monsoon anticyclone and of air masses found within the tropical pipe (6 months < age < 18 months).

Young air masses with an age lower than 6 months are found at the top of the Asian monsoon anticyclone up to altitudes of about 460 K by the end of August 2008. MIPAS satellite measurements of HCFC-22, a regional tracer emitted especially in continental eastern Asia and in the Near East, confirm our model result that young air masses from the region of the Asian monsoon are transported to the top of the anticyclone above the tropopause up to around 460 K.

A trajectory analysis in combination with the 3-dimensional CLaMS simulation shows that air masses from the lower troposphere are rapidly lofted by convective events up to approximately 360 K potential temperature (**convective range**) (see Fig. 13). Strong convection occurs both directly below the Asian monsoon anticyclone in India and China and outside the anticyclone region over Southeast Asia and the Pacific Ocean.

Above 360 K and up to ≈ 460 K, our findings from trajectory analysis demonstrate that air masses are uplifted in a anticyclonic large-scale upward spiral around the anticyclone extending from northern Africa to the western Pacific by diabatic heating of ≈ 1–1.5 K per day (**upward spiralling range**) (see Fig. 13). A straight homogeneous vertical cross-tropopause transport is not found in our backward trajectories, rather a very inhomogeneous horizontal distribution of tracers of air mass origin is found within and at the edge of the anticyclone, resulting in filamentary structures. Within the upward spiralling range strong horizontal transport of air masses from the eastern mode to the western mode of the anticyclone occurs. The altitude of the thermal tropopause is within this upward spiralling range. Thus, air masses in the upward spiral range are uplifted by diabatic heating across the (lapse rate) tropopause, which does not act as a transport barrier against this diabatic vertical transport process. Diabatic heating rates within the tropical transition layer have strong seasonal variability. Diabatic heating rates of up to ≈ 1 K per day – 1.5 K per day are in particular found between July and October 2008 over the region of the Asian monsoon anticyclone. In other regions within the tropical transition layer the heating rates are in general smaller (≈ 0.5–1.0 K per day).

Above 380 K mixing occurs between young air masses from inside (India/China) and outside (Southeast Asia / Pacific Ocean) the edge of the anticyclone. Between 420 K and 460 K highest contributions of young air masses are found around the edge of the anticyclone.

Thus, young air masses from the edge of the anticyclone originating in the tropical adjacent regions are mixed with air masses from inside the anticyclone mainly originating in India/China within the upward spiralling range above the anticyclone. Therefore, a significant fraction of air masses from the tropical adjacent regions is found within a widespread area around the anticyclone and above caused by the large-scale anticyclonic flow in this region, acting as a large-scale stirrer, which is consisted with our previous results (Vogel et al., 2014, 2016; Li et al., 2017).

Further between 420 K and 460 K, highest contributions from young air masses are found around the edge of the anticyclone, indicating a spatially strongly inhomogeneous ascent in the monsoon with strongest ascent at the edge. The higher in the upward spiralling range the more air masses from the stratospheric background are mixed with the young air masses transported upwards within this upward spiralling range.

To analyse the impact of air masses influenced by the region of the Asian monsoon on the composition of air masses within the tropical pipe at 550 K, the transport times from the Earth's surface up to this level of potential temperature need to be taken

Atmos. Chem. Phys. Discuss., https://doi.org/10.5194/acp-2018-724
Manuscript under review for journal Atmos. Chem. Phys.
Discussion started: 30 July 2018

into account. In a two-monsoon-season simulation tracing back air masses that are released at the Earth's surface since 1 May 2007 (age $<$ 18 months) only air masses older than 6 months are found within the tropical pipe at 550 K. Consequently, fresh emissions from the Asian monsoon season 2008 do not contribute to the distribution within the tropical pipe at 550 K. Air masses released during the monsoon season 2007 and during Winter 2007/2008 contribute up to 55% to the signal within the tropical pipe at 550 K. Air masses from India/China, mainly from inside the Asian monsoon anticyclone, contribute a minor fraction (6%) to the composition of air within the tropical pipe at 550 K; the major fraction is from Southeast Asia (16%) and the tropical Pacific (15%).

In summary, the transport pathway of air masses from the region of the Asian monsoon into the tropical pipe occurs in three distinct steps: first very fast uplift within the convective range up to $\approx$ 360 K within the Asian monsoon anticyclone and outside in the tropical adjacent regions (within a few days). Second, uplift above 360 K up to $\approx$ 460 K within the upward spiralling range (within a few months) and third above 460 K transport within the tropical pipe associated with the large-scale Brewer-Dobson circulation (within $\sim$ one year). Furthermore, we emphasise that in addition to air masses from within the Asian monsoon region air masses from the tropical adjacent regions (Southeast Asia/tropical Pacific/northern Africa/northwestern Pacific) are transported in a substantial percentage by this pathway into the tropical pipe.

Data availability. The complete MIPAS data are available at http://www.imk-asf.kit.edu/english/308.php.

Appendix A: Intraseasonal variability of upwelling above Asian monsoon anticyclone

Global 20-day backward trajectories are calculated at 360 K, 380 K, 400 K, 420 K, 440 K potential temperature on a $2.5° \times 2.0°$ longitude-latitude-grid from 1 June until 31 October 2008 covering the time period from monsoon-onset until post-monsoon to discuss the intraseasonal variability of upward transport at the top of the Asian monsoon anticyclone. Some chosen days (1 June, 1 July, 1 August, 1 September, and 1 October 2008) are shown in Fig. A1. During the monsoon season in July, August and September an upward transport of about 1–1.5 K per day is mainly found in the regions of the Asian monsoon anticyclone, in contrast to monsoon-onset in June. In June, an upward transport of about 1–1.5 K per day is found in the entire tropics, however the patterns are very inhomogeneous; in particular maximum values are found in the region of the northern subtropical jet stream.

Appendix B: Impact on the northern extratropical lower stratosphere

The accumulation of young air masses (age $<$ 6 months) from the region of the Asian monsoon since 1 May 2008 in the northern extratropical lower stratosphere is calculated using a climatological isentropic barrier derived by Kunz et al. (2015) that separates tropical tropospheric air from extra-tropical stratospheric air depending on potential temperature and season. To

calculate the percentages of different emission tracers within the lower extratropical stratosphere at 360 K and at 380 K, the mean value for each emission tracer of all CLaMS air parcels is calculated for PV values larger than those of the transport barrier (5.5 PVU at 360 K±0.5 K and 7.2 PVU at 380 K±0.5 K) and poleward of 30°N for each day between 1 May and 31 October 2008. Fig. A2 shows that at the end of October 2008, the contributions of young air masses to the composition of northern extratropical lower stratosphere is up to 48% at 360 K (up to 41% at 380 K not shown here). The contribution from India/China is up to 18% (16%) and from tropical Pacific and Southeast Asia up to 18% (16%).

Competing interests. The authors declare that they have no conflict of interest.

Acknowledgements. The authors sincerely thank Michael Volk (University Wuppertal), and William J. Randel (NCAR, Boulder) for very helpful discussions. We gratefully acknowledge the European Centre of Medium-Range Weather Forecasts (ECMWF) for providing the ERA-Interim reanalysis data. Our activities were partly funded by the European Community's Seventh Framework Programme (FP7/2007-2013) under the project StratoClim (grant agreement no. 603557) and by the German Science Foundation (Deutsche Forschungsgemeinschaft, DFG) under the DFG project AMOS (HALO-SPP 1294/VO 1276/5-1).

Atmos. Chem. Phys. Discuss., https://doi.org/10.5194/acp-2018-724
Manuscript under review for journal Atmos. Chem. Phys.
Discussion started: 30 July 2018

Atmospheric Chemistry and Physics Discussions

References

Annamalai, H. and Slingo, J. M.: Active/break cycles: diagnosis of the intraseasonal variability of the Asian Summer Monsoon, Clim. Dyn., 18, 85–102, 2001.

Bannister, R. N., O'Neill, A., Gregory, A. R., and Nissen, K. M.: The role of the south-east Asian monsoon and other seasonal features in creating the 'tape-recorder' signal in the Unified Model, Q. J. R. Meteorol. Soc., 130, 1531–1554, 2004.

Bergman, J. W., Jensen, E. J., Pfister, L., and Yang, Q.: Seasonal differences of vertical-transport efficiency in the tropical tropopause layer: On the interplay between tropical deep convection, large-scale vertical ascent, and horizontal circulations, J. Geophys. Res., 117, https://doi.org/10.1029/2011JD016992, 2012.

Bergman, J. W., Fierli, F., Jensen, E. J., Honomichl, S., and Pan, L. L.: Boundary layer sources for the Asian anticyclone: Regional contributions to a vertical conduit, J. Geophys. Res., 118, 2560–2575, https://doi.org/10.1002/jgrd.50142, 2013.

Bourassa, A. E., Robock, A., Randel, W. J., Deshler, T., Rieger, L. A., Lloyd, N. D., Llewellyn, E. J. T., and Degenstein, D. A.: Large Volcanic Aerosol Load in the Stratosphere Linked to Asian Monsoon Transport, Science, 337, 78–81, https://doi.org/10.1126/science.1219371, 2012.

Chirkov, M., Stiller, G. P., Laeng, A., Kellmann, S., von Clarmann, T., Boone, C. D., Elkins, J. W., Engel, A., Glatthor, N., Grabowski, U., Harth, C. M., Kiefer, M., Kolonjari, F., Krummel, P. B., Linden, A., Lunder, C. R., Miller, B. R., Montzka, S. A., Mühle, J., O'Doherty, S., Orphal, J., Prinn, R. G., Toon, G., Vollmer, M. K., Walker, K. A., Weiss, R. F., Wiegele, A., and Young, D.: Global HCFC-22 measurements with MIPAS: retrieval, validation, global distribution and its evolution over 2005-2012, Atmos. Chem. Phys., 16, 3345–3368, https://doi.org/10.5194/acp-16-3345-2016, www.atmos-chem-phys.net/16/3345/2016/, 2016.

Dee, D. P., Uppala, S. M., Simmons, A. J., Berrisford, P., Poli, P., Kobayashi, S., Andrae, U., Balmaseda, M. A., Balsamo, G., Bauer, P., Bechtold, P., Beljaars, A. C. M., van de Berg, L., Bidlot, J., Bormann, N., Delsol, C., Dragani, R., Fuentes, M., Geer, A. J., Haimberger, L., Healy, S. B., Hersbach, H., Holm, E. V., Isaksen, L., Kallberg, P., Koehler, M., Matricardi, M., McNally, A. P., Monge-Sanz, B. M., Morcrette, J.-J., Park, B.-K., Peubey, C., de Rosnay, P., Tavolato, C., Thepaut, J.-N., and Vitart, F.: The ERA-Interim reanalysis: configuration and performance of the data assimilation system, Q. J. R. Meteorol. Soc., 137, 553–597, https://doi.org/10.1002/qj.828, 2011.

Dethof, A., O'Neill, A., Slingo, J. M., and Smit, H. G. J.: A mechanism for moistening the lower stratosphere involving the Asian summer monsoon, Q. J. R. Meteorol. Soc., 556, 1079–1106, 1999.

Fadnavis, S., Schultz, M. G., Semeniuk, K., Mahajan, A. S., Pozzoli, L., Sonbawne, S., Ghude, S. D., Kiefer, M., and Eckert, E.: Trends in peroxyacetyl nitrate (PAN) in the upper troposphere and lower stratosphere over southern Asia during the summer monsoon season: regional impacts, Atmos. Chem. Phys., 14, 12 725–12 743, https://doi.org/10.5194/acp-14-12725-2014, 2014.

Fairlie, D., Vernier, J.-P., Natarajan, M., and Bedka, K. M.: Dispersion of the Nabro volcanic plume and its relation to the Asian summer monsoon, Atmos. Chem. Phys., 14, 7045–7057, https://doi.org/10.5194/acp-14-7045-2014, 2014.

Fischer, H., Birk, M., Blom, C., Carli, B., Carlotti, M., von Clarmann, T., Delbouille, L., Dudhia, A., Ehhalt, D., Endemann, M., Flaud, J. M., Gessner, R., Kleinert, A., Koopmann, R., Langen, J., López-Puertas, M., Mosner, P., Nett, H., Oelhaf, H., Perron, G., Remedios, J., Ridolfi, M., Stiller, G., , and Zander, R.: MIPAS: An instrument for atmospheric and climate resaerch, Atmos. Chem. Phys., 8, https://doi.org/10.5194/acp-8-2151-2008, 2008.

Fortems-Cheiney, A., Chevallier, F., Saunois, M., Pison, I., Bousquet, Cressot, C., Wang, H. J., Yokouchi, Y., and Artuso, F.: HCFC-22 emissions at global and regional scales between 1995 and 2010: Trends and variability, J. Geophys. Res., 118, 7379–7388, https://doi.org/10.1002/jgrd.50544, 2013.

Fromm, M., Kablick III, G., Nedoluha, G., Carboni, E., Grainger, R., Campbell, J., and Lewis, J.: Correcting the record of volcanic stratospheric aerosol impact: Nabro and Sarychev Peak, J. Geophys. Res., 119, 10 343–10 364, https://doi.org/10.1002/2014JD021507, http://dx.doi.org/10.1002/2014JD021507, 2014.

Garny, H. and Randel, W. J.: Dynamic variability of the Asian monsoon anticyclone observed in potential vorticity and correlations with tracer distributions, J. Geophys. Res., 118, 13 421–13 433, https://doi.org/10.1002/2013JD020908, 2013.

Garny, H. and Randel, W. J.: Transport pathways from the Asian monsoon anticyclone to the stratosphere, Atmos. Chem. Phys., 16, 2703–2718, https://doi.org/10.5194/acp-16-2703-2016, 2016.

Gill, A. E.: Some simple solutions for heat-induced tropical circulation, Q. J. R. Meteorol. Soc., 106, 447–462, 1980.

Glatthor, N., Höpfner, M., Stiller, G. P., , von Clarmann, T., Funke, B., Lossow, S., Eckert, E., Grabowski, U., Kellmann, S., Linden, A., Walker, K. A., and Wiegele, A.: Seasonal and interannual variations in HCN amounts in the upper troposphere and lower stratosphere observed by MIPAS, Atmos. Chem. Phys., 15, 563–582, https://doi.org/10.5194/acp-15-563-2015, 2015.

Griessbach, S., Hoffmann, L., Spang, R., von Hobe, M., Müller, R., and Riese, M.: MIPAS Volcanic Sulfate Aerosol Observations of the Nabro Eruption, in: Stratospheric Sulfur and its Role in Climate (SSiRC), Atlanta, Georgia, USA, October 2013, SPARC, http://www.sparc-ssirc.org/downloads/Griessbach.pdf, 2013.

Günther, G., Müller, R., von Hobe, M., Stroh, F., Konopka, P., and Volk, C. M.: Quantification of transport across the boundary of the lower stratospheric vortex during Arctic winter 2002/2003, Atmos. Chem. Phys., 8, 3655–3670, http://www.atmos-chem-phys.net/8/3655/2008/, 2008.

Highwood, E. J. and Hoskins, B. J.: The tropical tropopause, Q. J. R. Meteorol. Soc., 124, 1579 – 1604, 1998.

Höpfner, M., Volkamer, R., Grabowski, U., Grutter, M., Orphal, J., Stiller, G., von Clarmann, T., and Wetzel, G.: First detection of ammonia (NH_3) in the Asian summer monsoon upper troposphere, Atmos. Chem. Phys., 16, 14 357–14 369, https://doi.org/10.5194/acp-16-14357-2016, https://www.atmos-chem-phys.net/16/14357/2016/, 2016.

Hosking, J. S., Russo, M. R., Braesicke, P., and Pyle, J. A.: Tropical convective transport and the Walker circulation, Atmos. Chem. Phys., 12, 9791–9797, https://doi.org/10.5194/acp-12-9791-2012, https://www.atmos-chem-phys.net/12/9791/2012/, 2012.

Hossaini, R., Chipperfield, M., Montzka, M. P., Rap, S. A., Dhomse, S., and Feng, W.: Efficiency of short-lived halogens at influencing climate through depletion of stratopsheric ozone, Nature Geoscience, 8, 186–190, https://doi.org/10.1038/ngeo2363, 2015.

Hsu, C. J. and Plumb, R. A.: Nonaxisymmetric Thermally Driven Circulations and Upper-Tropospheric Monsoon Dynamics, J. Atmos. Sci., 57, 1255–1276, 2001.

Ko, M., Newman, P., Reimann, S., and Strahan, S., eds.: Lifetimes of Stratospheric Ozone-Depleting Substances, Their Replacements, and Related Species, SPARC Report No. 6, WCRP-15/2013, SPARC 6, 2013.

Konopka, P., Günther, G., Müller, R., dos Santos, F. H. S., Schiller, C., Ravegnani, F., Ulanovsky, A., Schlager, H., Volk, C. M., Viciani, S., Pan, L. L., McKenna, D.-S., and Riese, M.: Contribution of mixing to upward transport across the tropical tropopause layer (TTL), Atmos. Chem. Phys., 7, 3285–3308, 2007.

Konopka, P., Grooß, J.-U., Günther, G., Ploeger, F., Pommrich, R., Müller, R., and Livesey, N.: Annual cycle of ozone at and above the tropical tropopause: observations versus simulations with the Chemical Lagrangian Model of the Stratosphere (CLaMS), Atmos. Chem. Phys., 10, 121–132, https://doi.org/10.5194/acp-10-121-2010, http://www.atmos-chem-phys.net/10/121/2010/, 2010.

Konopka, P., Ploeger, F., and Müller, R.: Entropy- and static stability-based Lagrangian model grids, in: Geophysical Monograph Series: Lagrangian Modeling of the Atmosphere, edited by Lin, J., vol. 200, pp. 99–109, American Geophysical Union, https://doi.org/10.1029/2012GM001253, 2012.

Kumar, K. K., Rajagopalan, B., Hoerling, M., Bates, G., and Cane, M.: Unraveling the Mystery of Indian Monsoon Failure During El Niño, Science, 314, 115–119, https://doi.org/10.1126/science.1131152, 2006.

Kunz, A., Sprenger, M., and Wernli, H.: Climatology of potential vorticity streamers and associated isentropic transport pathways across PV gradient barriers, J. Geophys. Res., 120, 3802–3821, https://doi.org/10.1002/2014JD022615, http://dx.doi.org/10.1002/2014JD022615, 2014JD022615, 2015.

Li, D., Vogel, B., Bian, J., Müller, R., Pan, L. L., Günther, G., Bai, Z., Li, Q., Zhang, J., Fan, Q., and Vömel, H.: Impact of typhoons on the composition of the upper troposphere within the Asian summer monsoon anticyclone: the SWOP campaign in Lhasa 2013, Atmos. Chem. Phys., 17, 4657–4672, https://doi.org/10.5194/acp-17-4657-2017, https://www.atmos-chem-phys.net/17/4657/2017/, 2017.

Li, Q., Jiang, J. H., Wu, D. L., Read, W. G., Livesey, N. J., Waters, J. W., Zhang, Y., Wang, B., Filipiak, M. J., Davis, C. P., Turquety, S., Wu, S., Park, R. J., Yantosca, R. M., and Jacob, D. J.: Convective outflow of South Asian pollution: A global CTM simulation compared with EOS MLS observations, Geophys. Res. Lett., 32, L14 826, https://doi.org/10.1029/2005GL022762, 2005.

McKenna, D. S., Grooß, J.-U., Günther, G., Konopka, P., Müller, R., Carver, G., and Sasano, Y.: A new Chemical Lagrangian Model of the Stratosphere (CLaMS): 2. Formulation of chemistry scheme and initialization, J. Geophys. Res., 107, 4256, https://doi.org/10.1029/2000JD000113, 2002a.

McKenna, D. S., Konopka, P., Grooß, J.-U., Günther, G., Müller, R., Spang, R., Offermann, D., and Orsolini, Y.: A new Chemical Lagrangian Model of the Stratosphere (CLaMS): 1. Formulation of advection and mixing, J. Geophys. Res., 107, 4309, https://doi.org/10.1029/2000JD000114, 2002b.

Müller, S., Hoor, P., Bozem, H., Gute, E., Vogel, B., Zahn, A., Bönisch, H., Keber, T., Krämer, M., Rolf, C., Riese, M., Schlager, H., and Engel, A.: Impact of the Asian monsoon on the extratropical lower stratosphere: trace gas observations during TACTS over Europe 2012, Atmos. Chem. Phys., 16, 10 573–10 589, https://doi.org/10.5194/acp-16-10573-2016, 2016.

Nützel, M., Dameris, M., and Garny, H.: Movement, drivers and bimodality of the South Asian High, Atmos. Chem. Phys., 16, 14 755–14 774, https://doi.org/10.5194/acp-16-14755-2016, https://www.atmos-chem-phys.net/16/14755/2016/, 2016.

Orbe, C., Waugh, D. W., and Newman, P. A.: Air-mass origin in the tropical lower stratosphere: The influence of Asian boundary layer air, Geophys. Res. Lett., 42, 2015GL063937, https://doi.org/10.1002/2015GL063937, http://dx.doi.org/10.1002/2015GL063937, 2015.

Pan, L. L. and Munchak, L. A.: Relationship of cloud top to the tropopause and jet structure from CALIPSO data, J. Geophys. Res., 116, D12201, https://doi.org/10.1029/2010JD015462, 2011.

Pan, L. L., Konopka, P., and Browell, E. V.: Observations and model simulations of mixing near the extratropical tropopause, J. Geophys. Res., 111, D05106, https://doi.org/10.1029/2005JD006480, 2006.

Pan, L. L., Honomichl, S. B., Kinnison, D. E., Abalos, M., Randel, W. J., Bergman, J. W., and Bian, J.: Transport of chemical tracers from the boundary layer to stratosphere associated with the dynamics of the Asian summer monsoon, Journal of Geophysical Research: Atmospheres, 121, 14,159–14,174, https://doi.org/10.1002/2016JD025616, https://agupubs.onlinelibrary.wiley.com/doi/abs/10.1002/2016JD025616, 2016.

Park, M., Randel, W. J., Gettleman, A., Massie, S. T., and Jiang, J. H.: Transport above the Asian summer monsoon anticyclone inferred from Aura Microwave Limb Sounder tracers, J. Geophys. Res., 112, D16309, https://doi.org/10.1029/2006JD008294, 2007.

Park, M., Randel, W. J., Emmons, L. K., and Livesey, N. J.: Transport pathways of carbon monoxide in the Asian summer monsoon diagnosed from Model of Ozone and Related Tracers (MOZART), J. Geophys. Res., 114, D08303, https://doi.org/10.1029/2008JD010621, 2009.

Ploeger, F., Konopka, P., Günther, G., Grooß, J.-U., and Müller, R.: Impact of the vertical velocity scheme on modeling transport across the tropical tropopause layer, J. Geophys. Res., 115, D03301, https://doi.org/10.1029/2009JD012023, 2010.

Ploeger, F., Günther, G., Konopka, P., Fueglistaler, S., Müller, R., Hoppe, C., Kunz, A., Spang, R., Grooß, J.-U., and Riese, M.: Horizontal water vapor transport in the lower stratosphere from subtropics to high latitudes during boreal summer, J. Geophys. Res., 118, 8111–8127, https://doi.org/10.1002/jgrd.50636, 2013.

Ploeger, F., Gottschling, C., Grießbach, S., Grooß, J.-U., Günther, G., Konopka, P., Müller, R., Riese, M., Stroh, F., Tao, M., Ungermann, J., Vogel, B., and von Hobe, M.: A potential vorticity-based determination of the transport barrier in the Asian summer monsoon anticyclone, Atmos. Chem. Phys., 15, 13 145–13 159, https://doi.org/doi:10.5194/acp-15-13145-2015, 2015.

Ploeger, F., Konopka, P., Walker, K., and Riese, M.: Quantifying pollution transport from the Asian monsoon anticyclone into the lower stratosphere, Atmos. Chem. Phys., 17, 7055–7066, https://doi.org/10.5194/acp-17-7055-2017, https://www.atmos-chem-phys.net/17/7055/2017/, 2017.

Plumb, R. A.: A "tropical pipe" model of stratospheric transport, J. Geophys. Res., 101, 3957–3972, 1996.

Pommrich, R., Müller, R., Grooß, J.-U., Konopka, P., Ploeger, F., Vogel, B., Tao, M., Hoppe, C. M., Günther, G., Spelten, N., Hoffmann, L., Pumphrey, H.-C., Viciani, S., D'Amato, F., Volk, C. M., Hoor, P., Schlager, H., and Riese, M.: Tropical troposphere to stratosphere transport of carbon monoxide and long-lived trace species in the Chemical Lagrangian Model of the Stratosphere (CLaMS), Geosci. Model Dev., 7, 2895–2916, https://doi.org/10.5194/gmd-7-2895-2014, http://www.geosci-model-dev.net/7/2895/2014/, 2014.

Popovic, J. M. and Plumb, R. A.: Eddy Shedding from the Upper-Tropospheric Asian Monsoon Anticyclone, J. Atmos. Sci., 58, 93–104, 2001.

Randel, W. and Jensen, E.: Physical processes in the tropical tropopause layer and their role in a changing climate, Nature Geoscience, 6, 169–176, https://doi.org/10.1038/ngeo1733, 2013.

Randel, W. J. and Park, M.: Deep convective influence on the Asian summer monsoon anticyclone and associated tracer variability observed with Atmospheric Infrared Sounder (AIRS), J. Geophys. Res., 111, D12314, https://doi.org/10.1029/2005JD006490, 2006.

Randel, W. J., Park, M., Emmons, L., Kinnison, D., Bernath, P., Walker, K. A., Boone, C., and Pumphrey, H.: Asian Monsoon Transport of Pollution to the Stratosphere, Science, 328, 611–613, https://doi.org/10.1126/science.1182274, 2010.

Riese, M., Ploeger, F., Rap, A., Vogel, B., Konopka, P., Dameris, M., and Forster, P.: Impact of uncertainties in atmospheric mixing on simulated UTLS composition and related radiative effects, J. Geophys. Res., 117, D16305, https://doi.org/10.1029/2012JD017751, 2012.

Rolf, C., Vogel, B., Hoor, P., Afchine, A., Günther, G., Krämer, M., Müller, R., Müller, S., Spelten, N., and Riese, M.: Water vapor increase in the lower stratosphere of the Northern Hemisphere due to the Asian monsoon anticyclone observed during the TACTS/ESMVal campaigns, Atmospheric Chemistry and Physics, 18, 2973–2983, https://doi.org/10.5194/acp-18-2973-2018, https://www.atmos-chem-phys.net/18/2973/2018/, 2018.

Rosenlof, K. H., Tuck, A. F., Kelly, K. K., Russell III, J. M., and McCormick, M. P.: Hemispheric asymmetries in the water vapor and inferences about transport in the lower stratosphere, J. Geophys. Res., 102, 13 213–13 234, https://doi.org/10.1029/97JD00873, 1997.

Santee, M. L., Manney, G. L., Livesey, N. J., Schwartz, M. J., Neu, J. L., and Read, W. G.: A comprehensive overview of the climatological composition of the Asian summer monsoon anticyclone based on 10 years of Aura Microwave Limb Sounder measurements, Journal of Geophysical Research: Atmospheres, 122, 5491–5514, https://doi.org/10.1002/2016JD026408, https://agupubs.onlinelibrary.wiley.com/doi/abs/10.1002/2016JD026408, 2017.

Schoeberl, M. R., Dessler, A. E., and Wang, T.: Simulation of stratospheric water vapor and trends using three reanalyses, Atmos. Chem. Phys., 12, 6475–6487, https://doi.org/10.5194/acp-12-6475-2012, 2012.

Simmonds, P. G., Rigby, M., McCulloch, A., Vollmer, M. K., Henne, S., Mühle, J., O'Doherty, S., Manning, A. J., Krummel, P. B., Fraser, P. J., Young, D., Weiss, R. F., Salameh, P. K., Harth, C. M., Reimann, S., Trudinger, C. M., Steele, L. P., Wang, R. H. J., Ivy, D. J., Prinn,

R. G., Mitrevski, B., and Etheridge, D. M.: Recent increases in the atmospheric growth rate and emissions of HFC-23 (CHF_3) and the link to HCFC-22 ($CHClF_2$) production, Atmospheric Chemistry and Physics, 18, 4153–4169, https://doi.org/10.5194/acp-18-4153-2018, https://www.atmos-chem-phys.net/18/4153/2018/, 2018.

Solomon, S., Rosenlof, K., Portmann, R., Daniel, J., Davis, S., Sanford, T., and Plattner, G.-K.: Contributions of stratospheric water vapor to decadal changes in the rate of global warming, Science, 327, 1219–1223, https://doi.org/10.1126/science.1182488, 2010.

Spang, R., Günther, G., Riese, M., Hoffmann, L., Müller, R., and Griessbach, S.: Satellite observations of cirrus clouds in the Northern Hemisphere lowermost stratosphere, Atmospheric Chemistry and Physics, 15, 927–950, https://doi.org/10.5194/acp-15-927-2015, http://www.atmos-chem-phys.net/15/927/2015/, 2015.

Tissier, A.-S. and Legras, B.: Convective sources of trajectories traversing the tropical tropopause layer, Atmos. Chem. Phys., 16, 3383–3398, https://doi.org/10.5194/acp-16-3383-2016, 2016.

Uma, K. N., Das, S. K., and Das, S. S.: A climatological perspective of water vapor at the UTLS region over different global monsoon regions: observations inferred from the Aura-MLS and reanalysis data, Clim. Dyn., 43, 407–420, https://doi.org/10.1007/s00382-014-2085-9, 2014.

Ungermann, J., Ern, M., Kaufmann, M., Müller, R., Spang, R., Ploeger, F., Vogel, B., and Riese, M.: Observations of PAN and its confinement in the Asian summer monsoon anticyclone in high spatial resolution, Atmos. Chem. Phys., 16, 8389–8403, https://doi.org/10.5194/acp-16-8389-2016, 2016.

Vernier, J. P., Fairlie, T. D., Natarajan, M., Wienhold, F. G., Bian, J., Martinsson, B. G., Crumeyrolle, S., Thomason, L. W., and Bedka, K. M.: Increase in upper tropospheric and lower stratospheric aerosol levels and its potential connection with Asian pollution, J. Geophys. Res., https://doi.org/10.1002/2014JD022372, 2015.

Vogel, B., Konopka, P., Grooß, J.-U., Müller, R., Funke, B., López-Puertas, M., Reddmann, T., Stiller, G., von Clarmann, T., and Riese, M.: Model simulations of stratospheric ozone loss caused by enhanced mesospheric NO_x during Arctic Winter 2003/2004, Atmos. Chem. Phys., 8, 5279–5293, 2008.

Vogel, B., Pan, L. L., Konopka, P., Günther, G., Müller, R., Hall, W., Campos, T., Pollack, I., Weinheimer, A., Wei, J., Atlas, E. L., and Bowman, K. P.: Transport pathways and signatures of mixing in the extratropical tropopause region derived from Lagrangian model simulations, J. Geophys. Res., 116, D05306, https://doi.org/10.1029/2010JD014876, 2011.

Vogel, B., Günther, G., Müller, R., Grooß, J.-U., Hoor, P., Krämer, M., Müller, S., Zahn, A., and Riese, M.: Fast transport from Southeast Asia boundary layer sources to northern Europe: rapid uplift in typhoons and eastward eddy shedding of the Asian monsoon anticyclone, Atmos. Chem. Phys., 14, 12 745–12 762, https://doi.org/10.5194/acp-14-12745-2014, http://www.atmos-chem-phys.net/14/12745/2014/, 2014.

Vogel, B., Günther, G., Müller, R., Grooß, J.-U., and Riese, M.: Impact of different Asian source regions on the composition of the Asian monsoon anticyclone and of the extratropical lowermost stratosphere, Atmos. Chem. Phys., 15, 13 699–13 716, https://doi.org/10.5194/acp-15-13699-2015, http://www.atmos-chem-phys.net/15/13699/2015/, 2015.

Vogel, B., Günther, G., Müller, R., Jens-Uwe Grooß, A. A., Bozem, H., Hoor, P., Krämer, M., Müller, S., Riese, M., Rolf, C., Spelten, N., Stiller, G. P., Ungermann, J., and Zahn, A.: Long-range transport pathways of tropospheric source gases originating in Asia into the northern lower stratosphere during the Asian monsoon season 2012, Atmos. Chem. Phys., 16, 15 301–15 325, https://doi.org/10.5194/acp-16-15301-2016, http://www.atmos-chem-phys.net/16/15301/2016/, 2016.

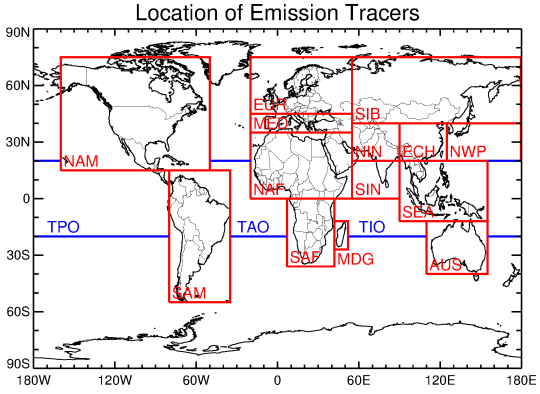

Figure 1. Global geographical location of artificial boundary layer source regions in the CLaMS model, also referred to as 'emission tracers' adapted from Vogel et al. (2015). The latitude and longitude range for each emission tracer is listed in Table 1.

Volk, C. M., Elkins, J. W., Fahey, D. W., Salawitch, R. J., Dutton, G. S., Gilligan, J. M., Proffitt, M. H., Loewenstein, M., Podolske, J. R., Minschwaner, K., Margitan, J. J., and Chan, K. R.: Quantifying transport between the tropical and mid-latitude lower stratosphere, Science, 272, 1763–1768, 1996.

Webster, P. J., Magaña, V. O., Palmer, T. N., Shukla, J., Tomas, R. A., Yanai, M., and Yasunari, T.: Monsoon: Processes, predictability, and the prospects for prediction, J. Geophys. Res., 103, 14.451–14.510, 1998.

Wright, J. S. and Fueglistaler, S.: Large differences in reanalyses of diabatic heating in the tropical upper troposphere and lower stratosphere, Atmos. Chem. Phys., 13, 9565–9576, https://doi.org/10.5194/acp-13-9565-2013, 2013.

Wu, X., Griessbach, S., and Hoffmann, L.: Equatorward dispersion of a high-latitude volcanic plume and its relation to the Asian summer monsoon: a case study of the Sarychev eruption in 2009, Atmos. Chem. Phys., 17, 13 439–13 455, https://doi.org/10.5194/acp-17-13439-2017, https://www.atmos-chem-phys.net/17/13439/2017/, 2017.

Zhang, Q., Wu, G., and Qian, Y.: The Bimodality of the 100 hPa South Asia High and its Relationship to the Climate Anomaly over East Asia in Summer, J. Meteorol. Soc. Jpn., 80, 733–744, 2002.

Atmos. Chem. Phys. Discuss., https://doi.org/10.5194/acp-2018-724
Manuscript under review for journal Atmos. Chem. Phys.
Discussion started: 30 July 2018

Atmospheric Chemistry and Physics Discussions

Table 1. Latitude and longitude range of artificial boundary layer sources in the CLaMS model, also referred to as "emission tracers". The geographical position of each emission tracer is shown in Fig. 1 (adapted from Vogel et al. (2015, 2016))

Emission tracer	Latitude	Longitude
Northern India (NIN)	20–40° N	55–90° E
Southern India (SIN)	0–20° N	55–90° E
Eastern China (ECH)	20–40° N	90–125° E
Southeast Asia (SEA)	12° S–20° N	90–155° E
Northwestern Pacific (NWP)	20–40° N	125–180° E
Siberia (SIB)	40–75° N	55–180° E
Europe (EUR)	45–75° N	20° W–55° E
Mediterranean (MED)	35–45° N	20° W–55° E
Northern Africa (NAF)	0–35° N	20° W–55° E
Southern Africa (SAF)	36° S–0° N	7–42° E
Madagascar (MDG)	27–12° S	42–52° E
Australia (AUS)	40–12° S	110–155° E
North America (NAM)	15–75° N	160–50° W
South America (SAM)	55° S–15° N	80–35° W
Tropical Pacific Ocean (TPO)	20° S–20° N	see Fig. 1
Tropical Atlantic Ocean (TAO)	20° S–20° N	see Fig. 1
Tropical Indian Ocean (TIO)	20° S–20° N	see Fig. 1
India/China	NIN+SIN+ECH	
tropical adjacent regions (TAR)	SEA+TPO+NAF+NWP	
ALL	entire surface	

Atmos. Chem. Phys. Discuss., https://doi.org/10.5194/acp-2018-724
Manuscript under review for journal Atmos. Chem. Phys.
Discussion started: 30 July 2018

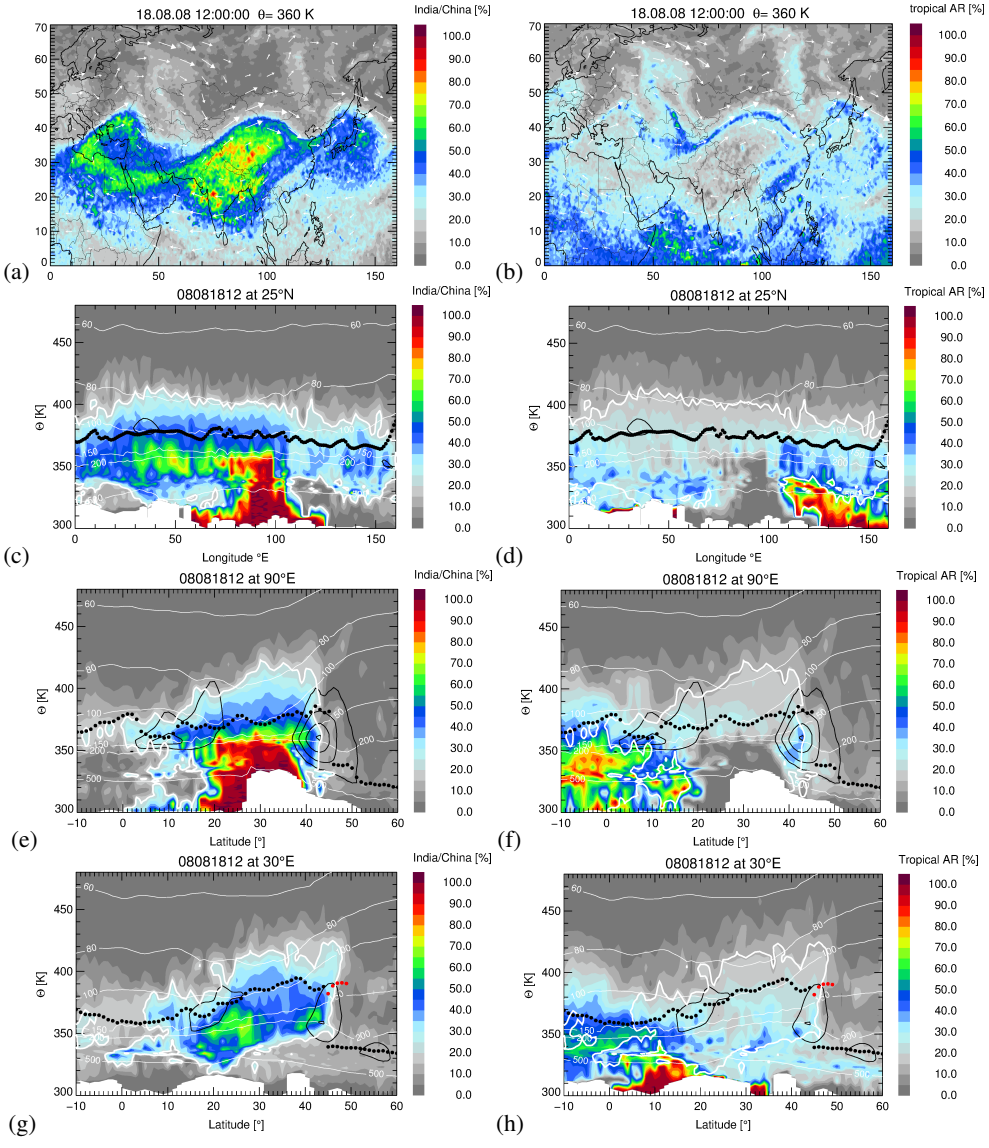

Figure 2. Horizontal distribution of the fraction of air originating in India/China (left) and in tropical adjacent regions (right) at 360 K potential temperature, longitude–theta cross sections at 25°N and latitude–theta cross sections at 90°E (eastern part of the anticyclone) and 30°E (western part of the anticyclone) on 18 August 2008. The horizontal winds are indicated by white arrows (maps) or by black thin lines (cross sections) (shown are 30, 40, 50, and 60 m/s). The first thermal tropopause is marked by black dots, the second thermal tropopause by red dots, and the corresponding levels of pressure are marked by thin white lines. The contour line of 20% percentages of the India/China tracer is shown by thick white lines.

Atmos. Chem. Phys. Discuss., https://doi.org/10.5194/acp-2018-724
Manuscript under review for journal Atmos. Chem. Phys.
Discussion started: 30 July 2018

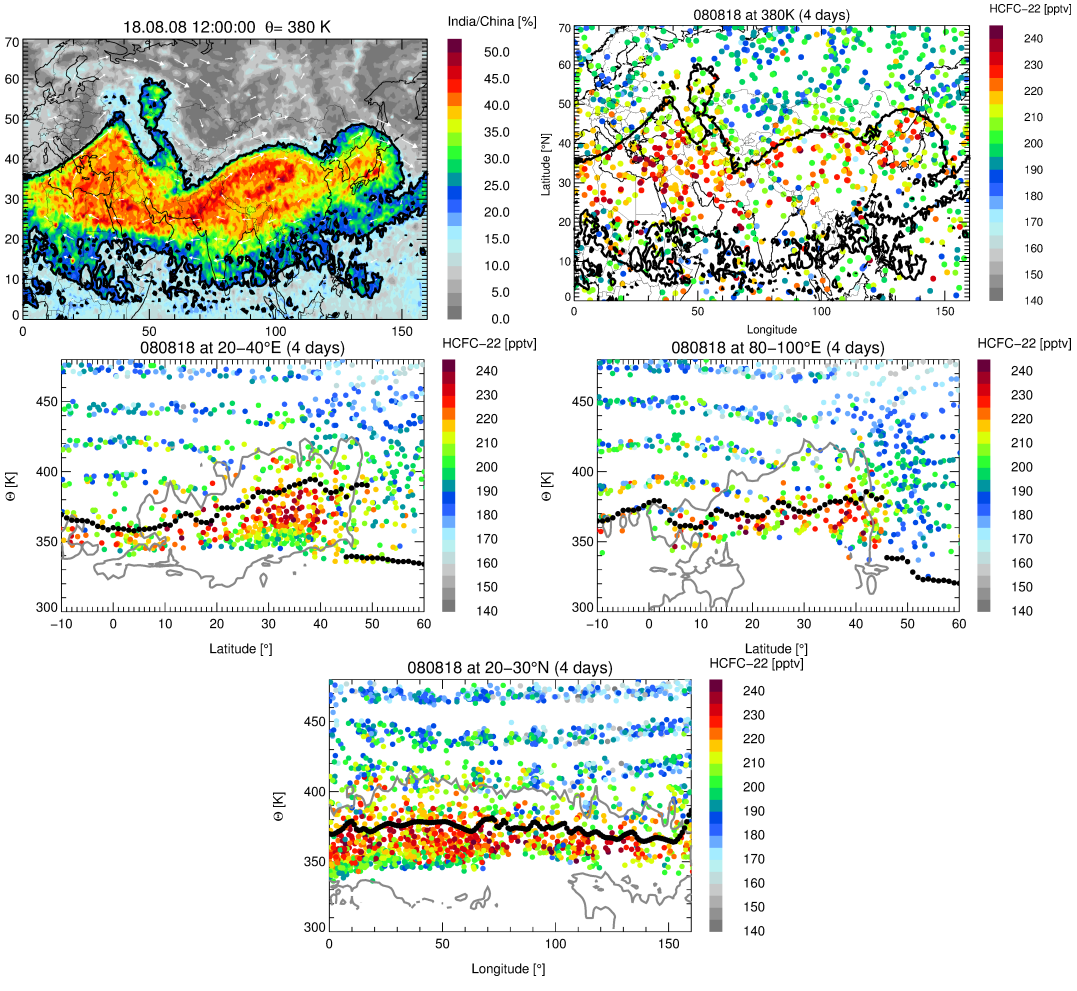

Figure 3. Horizontal distribution of the fraction of air originating in India/China (left) and of MIPAS HCFC-22 measurements (right) at 380 K potential temperature (top). The MIPAS measurements are synoptically interpolated within 4 days (for details see Sect. 2.4). Latitude–theta cross sections at 30°E (western part of the anticyclone) and 90°E (eastern part of the anticyclone) on 18 August 2008 are shown (2nd row) as well as a longitude–theta cross section at 25°N (bottom). The contour line of 20% of the India/China tracer is shown by thick black or grey lines as shown in Fig. 2.

Atmos. Chem. Phys. Discuss., https://doi.org/10.5194/acp-2018-724
Manuscript under review for journal Atmos. Chem. Phys.
Discussion started: 30 July 2018

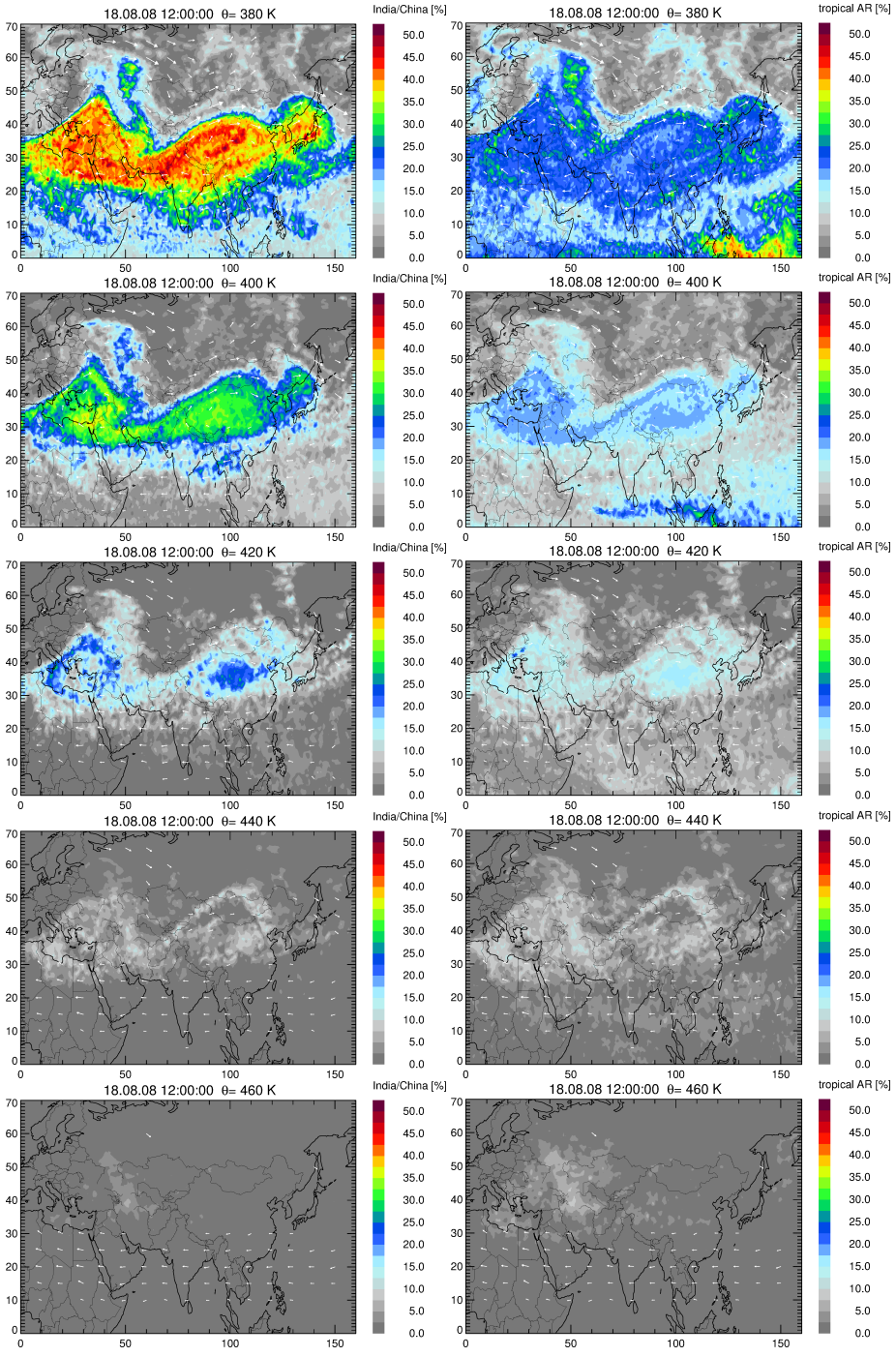

Figure 4. Horizontal distribution of the fraction of air originating in India/China (left) and in tropical adjacent regions (right) at 380 K, 400 K, 420 K, 440 K, and 460 K potential temperature.

Atmos. Chem. Phys. Discuss., https://doi.org/10.5194/acp-2018-724
Manuscript under review for journal Atmos. Chem. Phys.
Discussion started: 30 July 2018

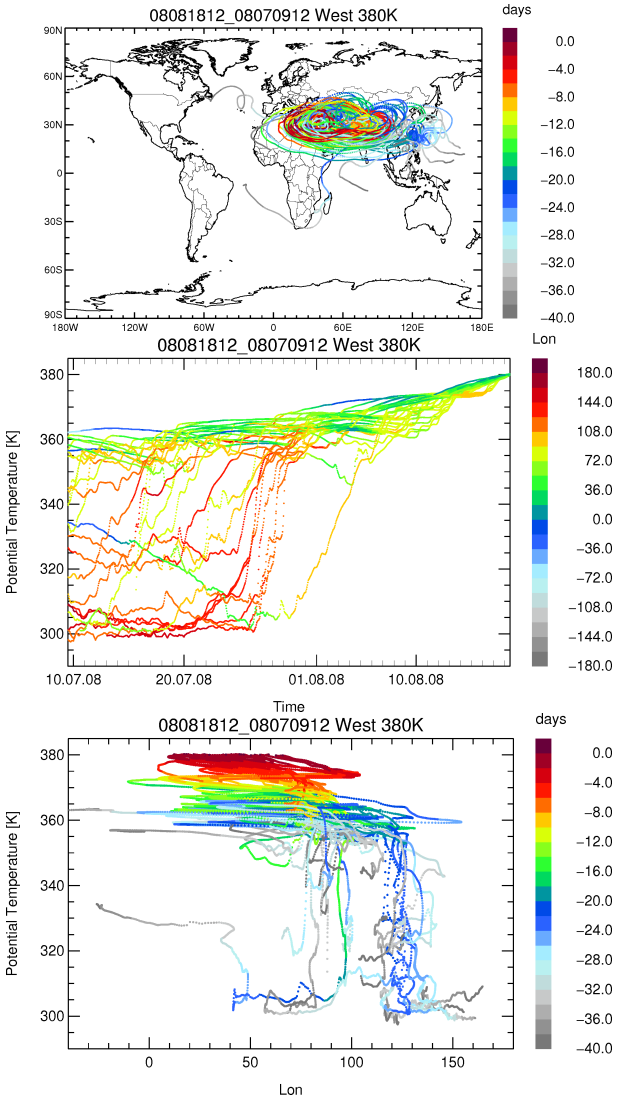

Figure 5. Different 40-day backward trajectories started at 380 K in the western mode of the Asian monsoon anticyclone are shown colour-coded by days back from 18 August 2008 (top). Further, potential temperature versus time (in UTC) along 40-day backward trajectories colour-coded by longitude (middle) and potential temperature versus longitude colour-coded by days reversed from 18 August 2008 (bottom) are shown. The trajectory positions are plotted every hour (coloured dots). Large distances between single positions indicate rapid uplift.

Atmos. Chem. Phys. Discuss., https://doi.org/10.5194/acp-2018-724
Manuscript under review for journal Atmos. Chem. Phys.
Discussion started: 30 July 2018

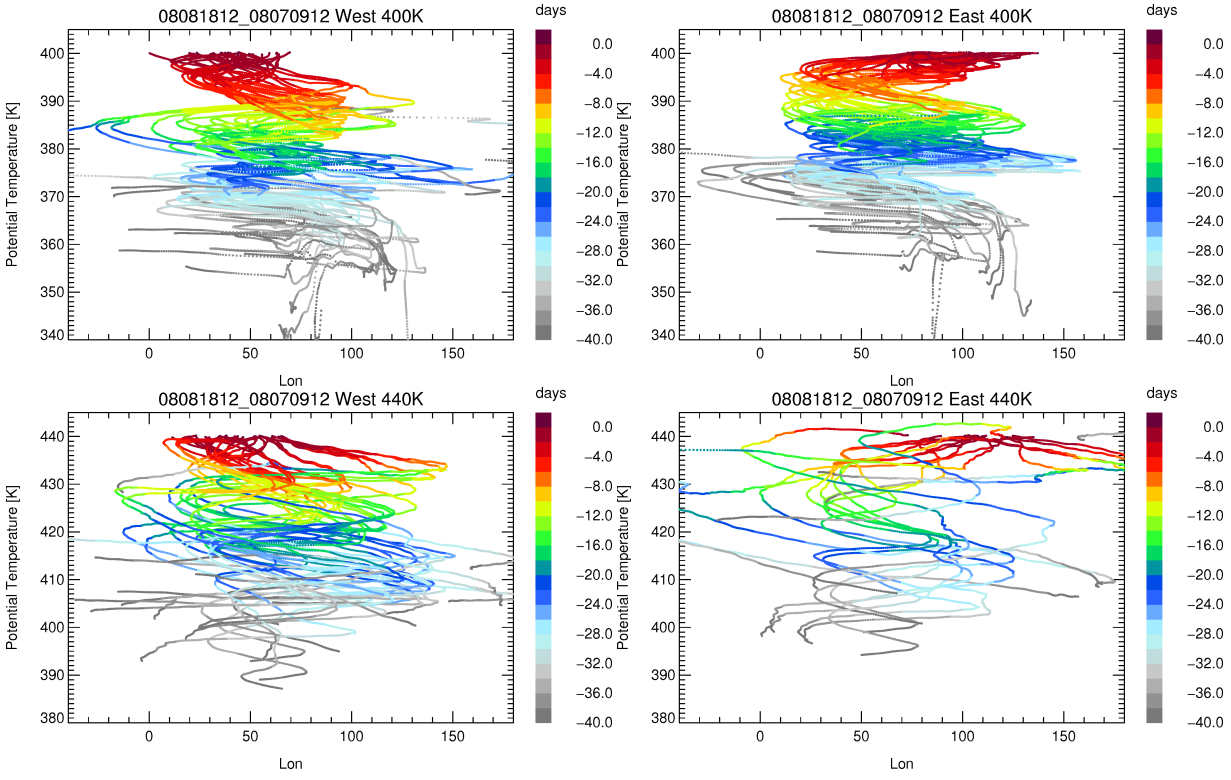

Figure 6. Potential temperature of different 40-day backward trajectories started at 400 K (top) and 440 K (bottom) in the western (left) and eastern mode (right) of the Asian monsoon anticyclone are shown versus longitude colour-coded by days reversed from 18 August 2008

Atmos. Chem. Phys. Discuss., https://doi.org/10.5194/acp-2018-724
Manuscript under review for journal Atmos. Chem. Phys.
Discussion started: 30 July 2018

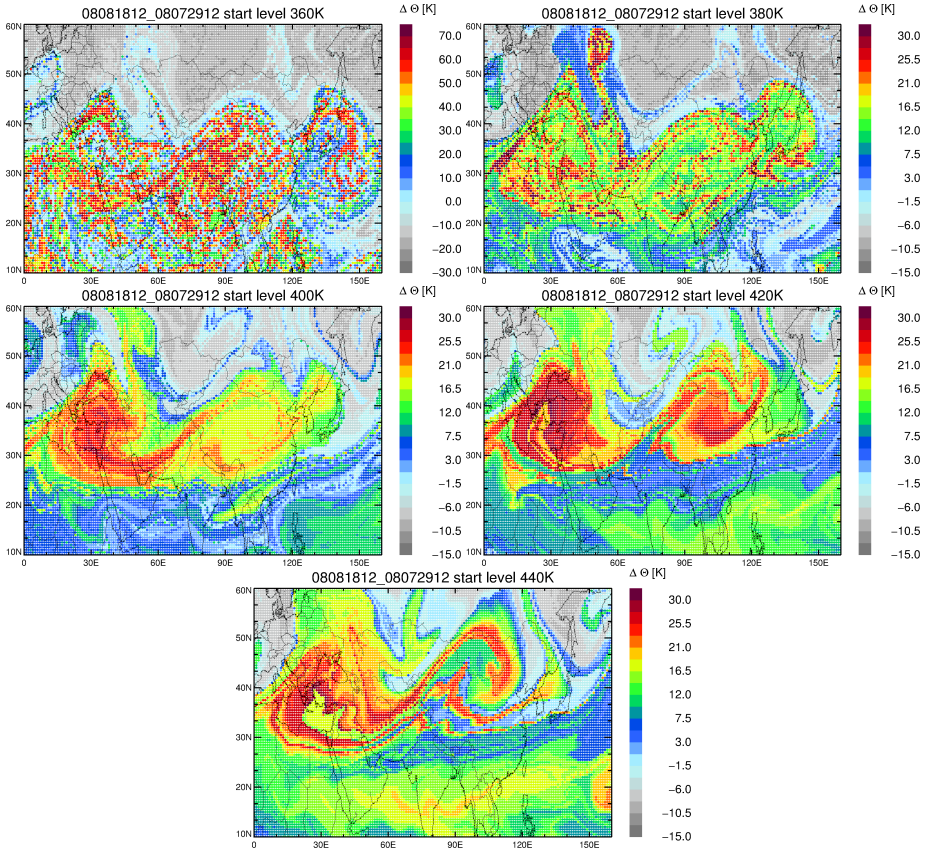

Figure 7. The change in potential temperature ($\Delta\Theta$) along 20-day backward trajectories initialised on 18 August 2008 are shown for different levels of potential temperature (360 K, 380 K, 400 K, 420 K, and 440 K). Note that the range of the colour bar in the 1st row is much larger than in the other rows. At the lower potential temperature levels (360 K, 380 K), some 20-day backward trajectories exist that reach the model boundary layer within a time period shorter than 20 days (in cases of very strong uplift by convection). For these trajectories $\Delta\Theta$ is shown for the shorter time period.

Atmos. Chem. Phys. Discuss., https://doi.org/10.5194/acp-2018-724
Manuscript under review for journal Atmos. Chem. Phys.
Discussion started: 30 July 2018

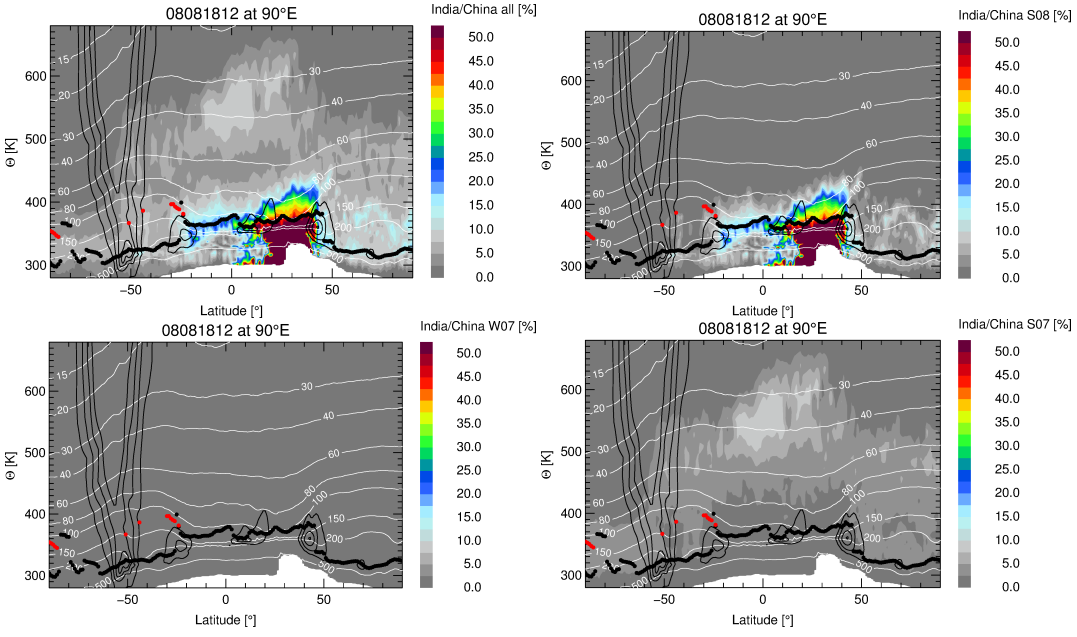

Figure 8. Latitude–theta cross sections at 90°E for the fraction of the India/China tracer for the entire simulation period (1 May 2007 - 31 October 2008 labeled as 'all'), for the Summer 08 (S08) pulse, for the Winter 07/08 (W07) pulse, and for the Summer 07 (S07) pulse on 18 August 2008. The thermal tropopause (first in black dots and second in red dots) and horizontal winds (black lines) are shown. The corresponding levels of pressure are marked by thin white lines.

Atmos. Chem. Phys. Discuss., https://doi.org/10.5194/acp-2018-724
Manuscript under review for journal Atmos. Chem. Phys.
Discussion started: 30 July 2018

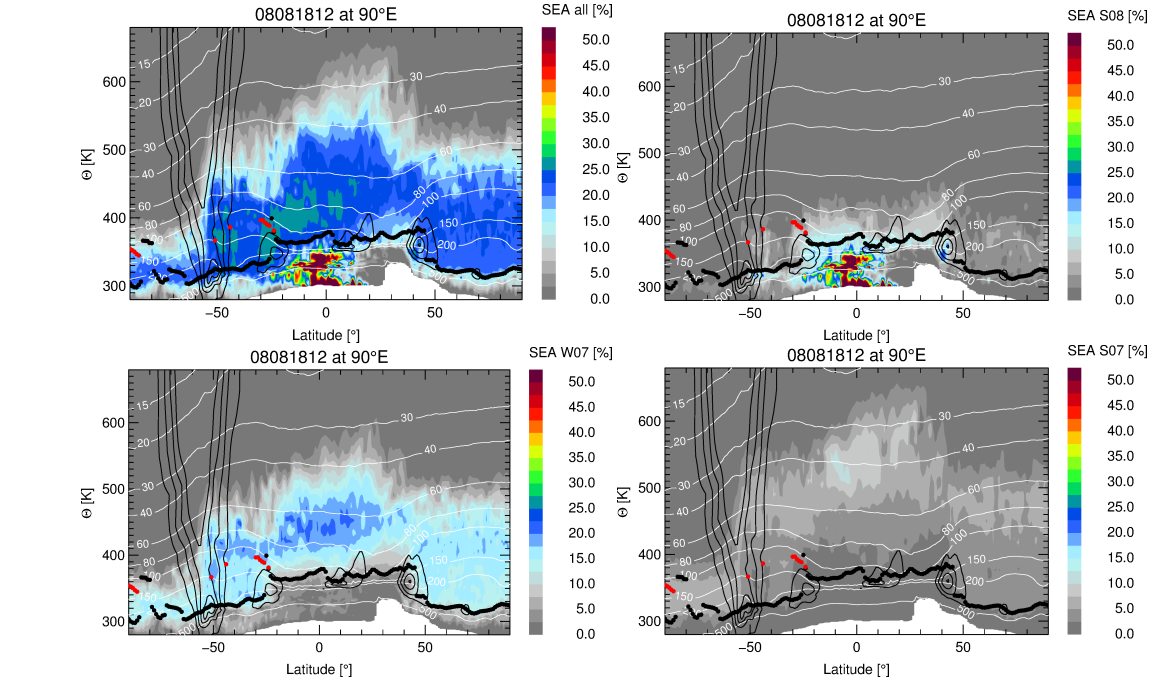

Figure 9. As Fig. 8 but for the fraction of the tracer for Southeast Asia (SEA)

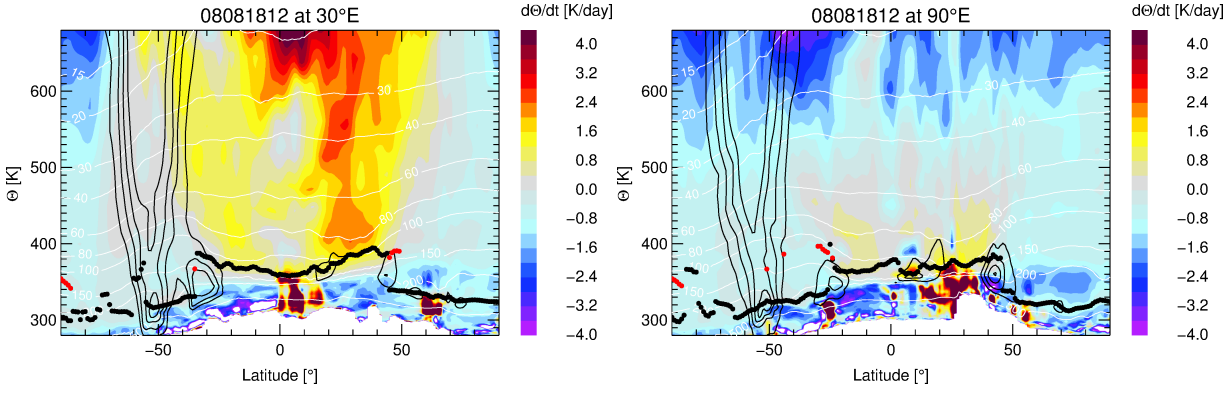

Figure 10. Latitude–theta cross section of dΘ/dt showing the radiative heating above the Asian monsoon anticyclone for the western (30°E) and eastern mode (90°E) of the anticyclone on 18 August 2008. The thermal tropopause (first in black dots and second in red dots) and horizontal winds (black lines) are shown. The corresponding levels of pressure are marked by thin white lines.

Atmos. Chem. Phys. Discuss., https://doi.org/10.5194/acp-2018-724
Manuscript under review for journal Atmos. Chem. Phys.
Discussion started: 30 July 2018

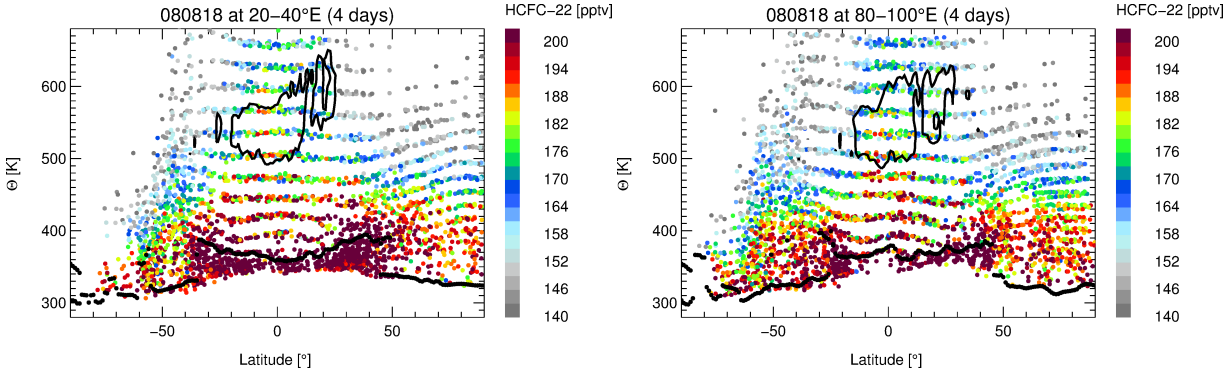

Figure 11. Latitude–theta cross sections of MIPAS HCFC-22 measurements crossing the western (20°E-40°E) and eastern mode (80°E-100°E) of the anticyclone up to 680 K potential temperature on 18 August 2008. The thermal tropopause is indicated by black dots. The contour line of 6% of the India/China tracer for the Summer 07 pulse is shown by thick black lines as shown in Fig. 8. To highlight the MIPAS HCFC-22 signal within the tropical pipe the plot range of the data is up to 200 pptv. Note that the maximum values of MIPAS HCFC-22 in the troposphere are higher than 200 pptv.

Atmos. Chem. Phys. Discuss., https://doi.org/10.5194/acp-2018-724
Manuscript under review for journal Atmos. Chem. Phys.
Discussion started: 30 July 2018

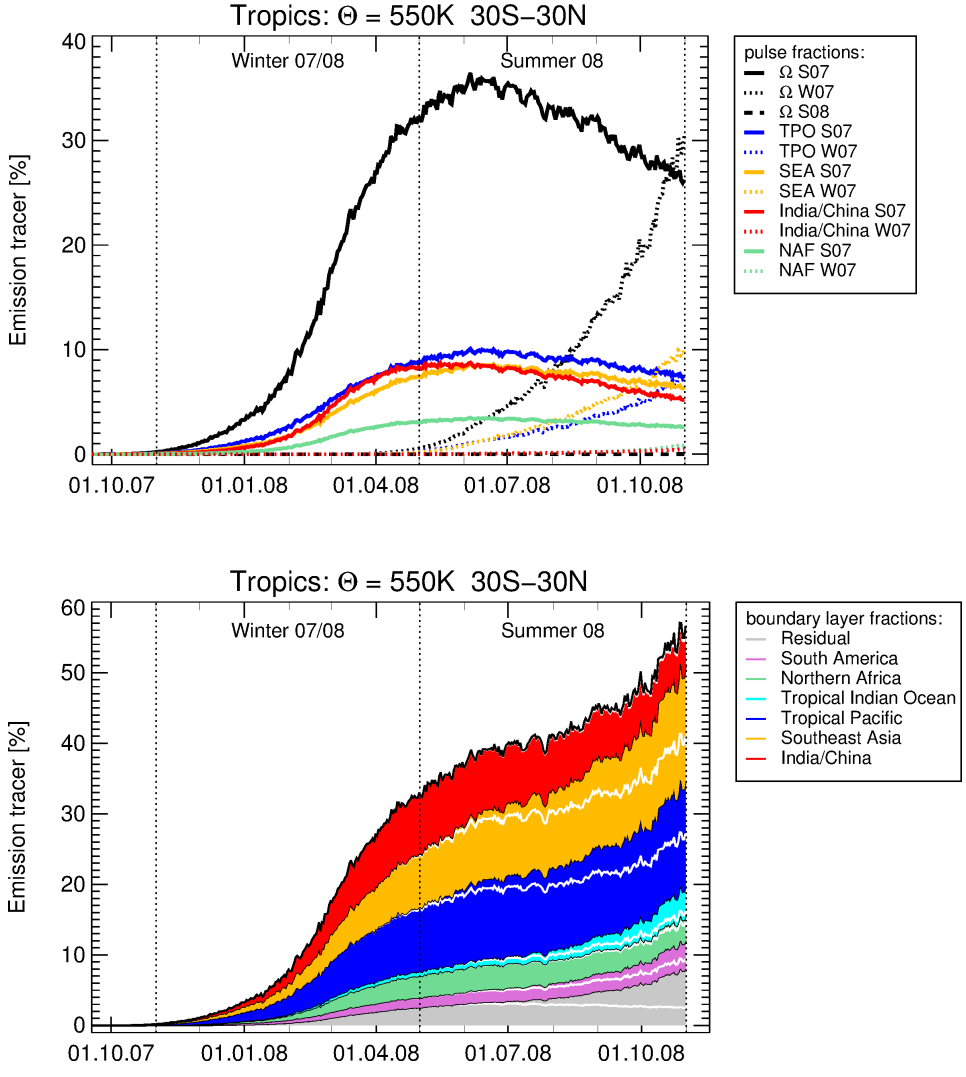

Figure 12. The contribution of the three different time pulses S07, W07, and S08 (each set for a time period of 6 months) for the entire Earth's surface (Ω_{S07}, Ω_{W07}, Ω_{S08}) to the tropical pipe between 30°S and 30°N at 550 K potential temperature from 1 October 2007 until the end of the simulation period (31 October 2008) (top, black lines). Emission tracers released during S08 have no contribution to the tropical pipe at 550 K. The contribution of several tracers of air mass origin to the individual pulses are shown in colours .

Contribution of different emission tracers for the tropical Pacific Ocean, Southeast Asia, India/China, South America, Northern Africa, tropical Indian Ocean, and the residual surface (all other regions of the Earth's surface) to the tropical pipe between 30°S and 30°N at 550 K potential temperature from 1 October 2007 until the end of the simulation period (bottom). The contribution of the three time pulses for the different emission tracers are marked by thin white lines for S07 and by thin black lines for W07.

Atmos. Chem. Phys. Discuss., https://doi.org/10.5194/acp-2018-724
Manuscript under review for journal Atmos. Chem. Phys.
Discussion started: 30 July 2018

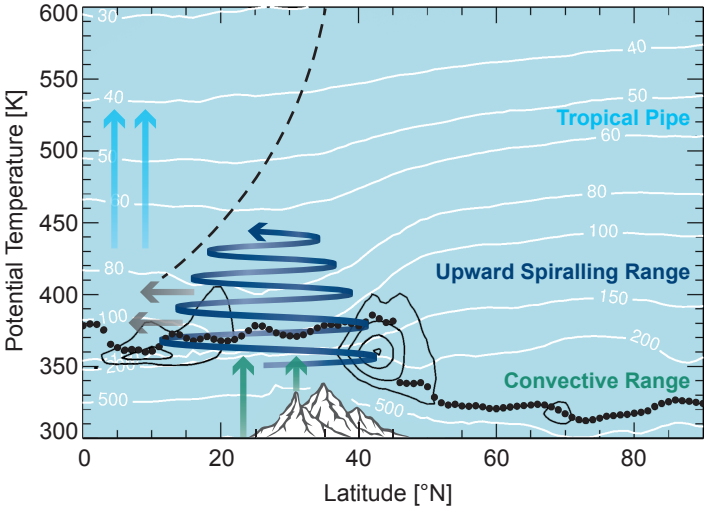

Figure 13. The transport pathway of air masses from the region of the Asian monsoon into the tropical pipe occurs in three distinct steps: first very fast uplift within the convective range up to ≈ 360 K within the Asian monsoon anticyclone and outside in the tropical adjacent regions (within a few days). Second, uplift above 360 K (up to ≈ 460 K) within the upward spiralling range (within a few months) and third transport within the tropical pipe to altitudes higher than 460 K associated with the large-scale Brewer-Dobson circulation (within ∼ one year). The thermal tropopause (black dots) and horizontal winds (black lines) are shown. The corresponding levels of pressure are marked by thin white lines. Large grey arrows indicate isentropic transport from the Asian monsoon anticyclone into the tropics.

Atmos. Chem. Phys. Discuss., https://doi.org/10.5194/acp-2018-724
Manuscript under review for journal Atmos. Chem. Phys.
Discussion started: 30 July 2018

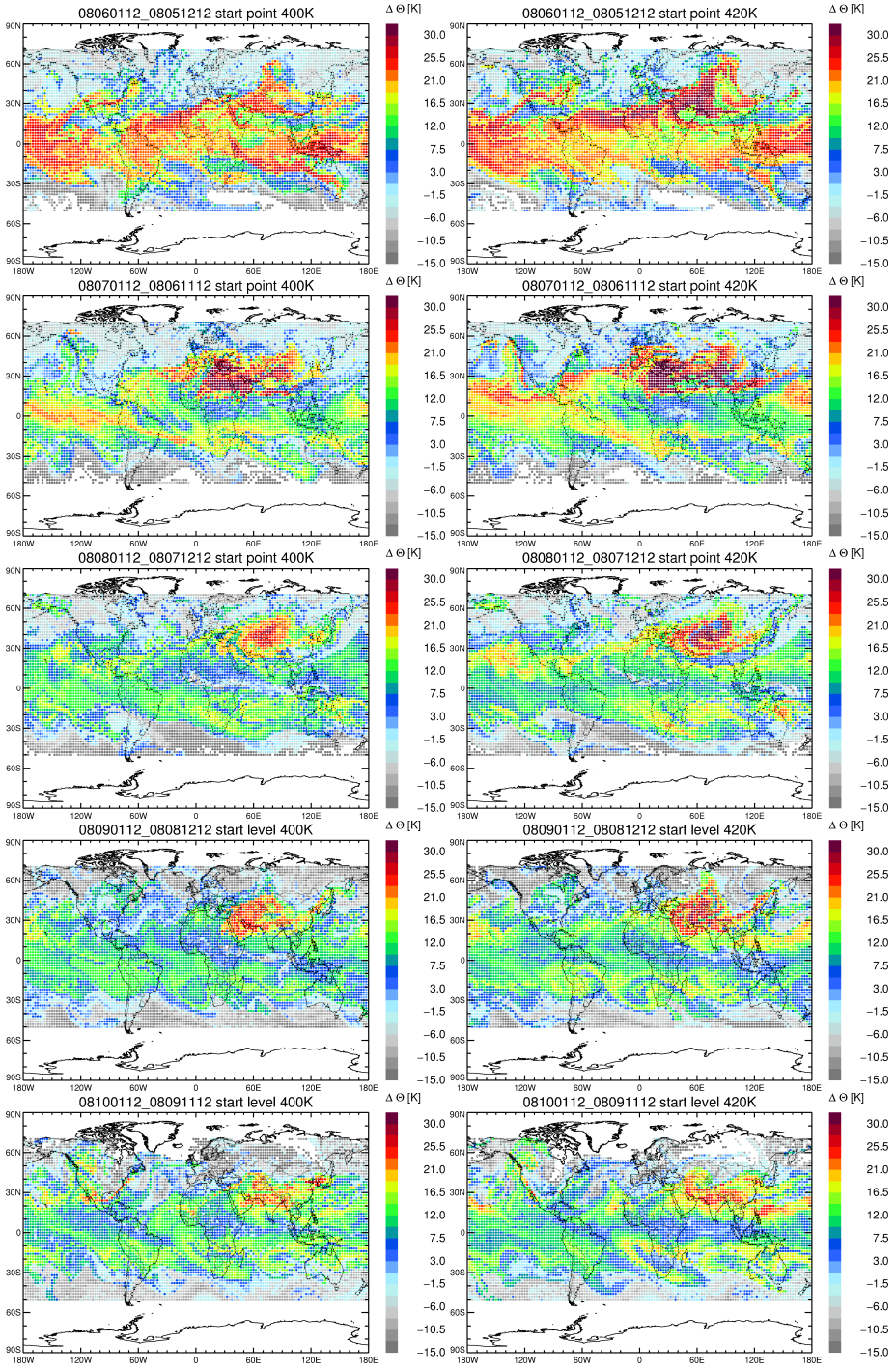

Figure A1. The change in potential temperature ($\Delta\Theta$) along 20-day backward trajectories initialised on 18 August 2008 are shown for different levels of potential temperature (400 K and 420 K) for different days from monsoon-onset until post-monsoon (1st June, 1st July, 1st August, 1st September, and 1st October 2008).

Atmos. Chem. Phys. Discuss., https://doi.org/10.5194/acp-2018-724
Manuscript under review for journal Atmos. Chem. Phys.
Discussion started: 30 July 2018

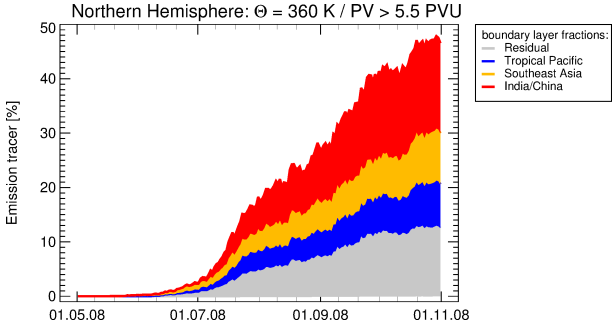

Figure A2. Contribution of different emission tracers from India/China, southeast Asia, the tropical Pacific Ocean, and residual surface to the northern lower stratosphere at 360 K from May to October 2008.